iScience

CellPress
OPEN ACCESS

Article

Chemoproteomics reveals berberine directly binds to PKM2 to inhibit the progression of colorectal cancer

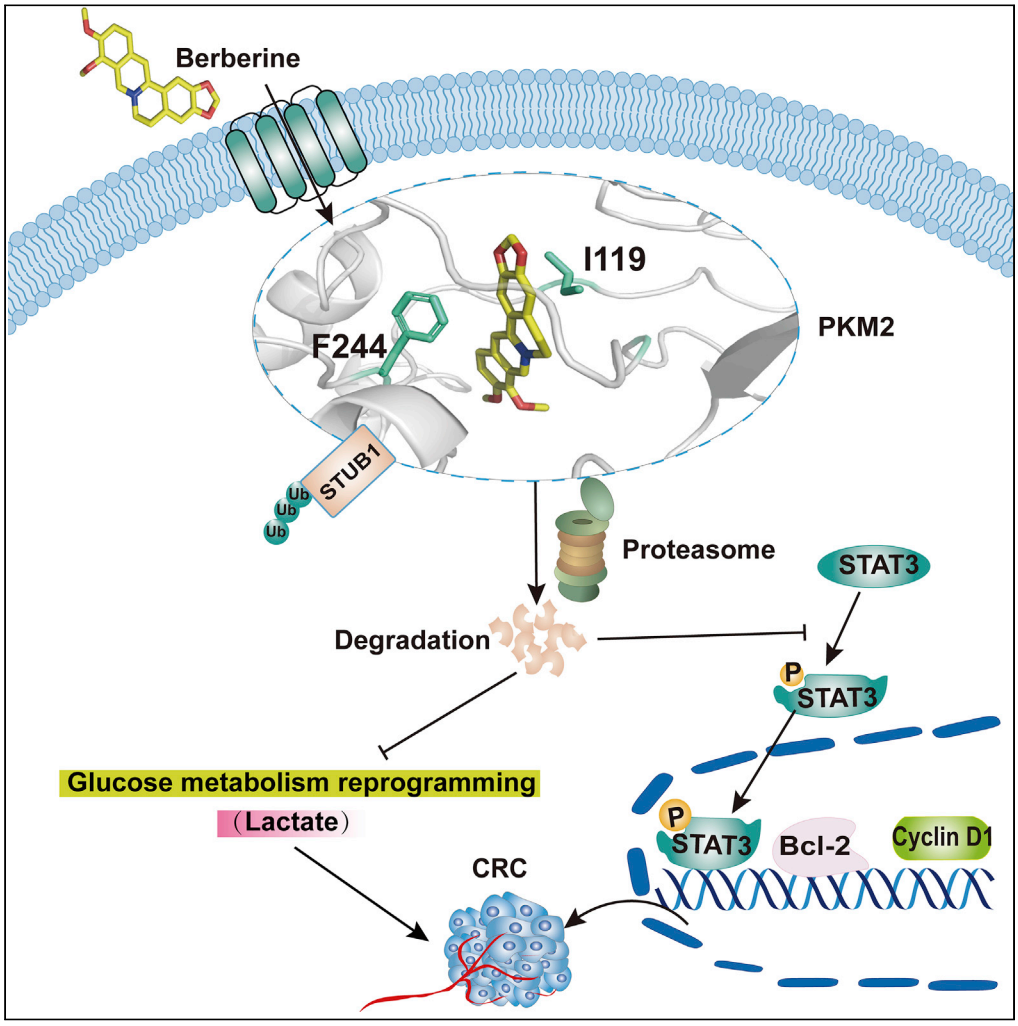

Shi-Hai Yan, Li-Mu Hu, Xue-Hui Hao, ..., Zhi-Rong Geng, Jing Ma, Zhi-Lin Wang

gengzr@nju.edu.cn (Z.-R.G.)
majing@nju.edu.cn (J.M.)
wangzl@nju.edu.cn (Z.-L.W.)

Highlights

Berberine directly targets PKM2 to inhibit colorectal cancer

Berberine forms hydrophobic interaction with I119 and π-π interaction with F244 of PKM2

P-aminobenzoic acid-berberine ester was synthesized to improve the biological activity

Yan et al., iScience 25, 104773
August 19, 2022
https://doi.org/10.1016/j.isci.2022.104773

iScience

CellPress
OPEN ACCESS

Article

Chemoproteomics reveals berberine directly binds to PKM2 to inhibit the progression of colorectal cancer

Shi-Hai Yan,[1,2] Li-Mu Hu,[1] Xue-Hui Hao,[1] Jiang Liu,[2] Xi-Ying Tan,[2] Zhi-Rong Geng,[1,3,*] Jing Ma,[1,*] and Zhi-Lin Wang[1,*]

SUMMARY

Colorectal cancer is one of the most serious tumors and berberine can inhibit the recurrence and transformation of colorectal adenoma into colorectal cancer. However, the direct binding target proteins of berberine in inhibiting colorectal cancer remain unclear. In this study, the chemical proteomics method was used and demonstrated that berberine is directly bound to pyruvate kinase isozyme type M2 (PKM2) in colorectal cancer cells. The triangular N-*O*-O triangular structure of berberine contributed to hydrophobic interaction with I119 amino acid residues and π-π interaction with F244 amino acid residues of PKM2 protein. Moreover, berberine was shown to inhibit the reprogramming of glucose metabolism and the phosphorylation of STAT3, down regulate the expression of Bcl-2 and Cyclin D1 genes, ultimately inhibiting the progression of colorectal cancer. This study uncovered the direct binding target protein and mechanism of berberine to improve metabolic reprogramming in colorectal cancer, which is helpful to guide the optimization of berberine.

INTRODUCTION

Colorectal cancer is currently the third most prevalent malignancy and second most deadly cancer worldwide (Bray et al., 2018). The outcome is still unsatisfactory despite using various treatments such as surgery, chemotherapy, and radiotherapy. Drug research has mainly focused on preventing the occurrence of colorectal cancer in high-risk populations and recurrence in post-operative patients, and improving outcomes in patients with advanced disease. Given the side effect profile and limitations in improving the prognosis of existing treatments, there remains an unmet medical need for alternative options, such as medicinal plants, in the treatment of colorectal cancer.

Berberine, a quaternary ionic isoquinoline alkaloid (Figure 1A), is the main active ingredient of the medicinal plants Huang Lian and Huang Bai and has antibacterial, diarrheal, hypolipidemic, and hypoglycemic effects (Chen et al., 2015; Zhang et al., 2008; Kong et al., 2004). In recent years, *Lancet Gastroenterol Hepatol* has reported that berberine could reduce colorectal adenoma recurrence and inhibit colorectal carcinogenesis for the chemoprevention of colorectal adenoma and intestinal cancer (Chen et al., 2020b; Kwon and Chan, 2020).

The molecular mechanisms of berberine have been initially explored in several studies, involving the inhibition of the expression of the oncogenes C-MYC and hypoxia-inducible factor HIF-1 in colorectal cancer cells (Mao et al., 2018), reduction of the transcription of the glucose uptake and glucose metabolism genes GLUT1, LDHA and HK2 (Wu et al., 2018), activation of AMPK signaling to inhibit the expression of cyclooxygenase (COX-2) (Li et al., 2015), inhibition of GTPase ERAL1 and mitochondrial ribosomal proteins including MRPL11, 15, 30, 37, 40, and 52 in colorectal cancer cells (Li et al., 2021a). In addition, berberine could stabilize the structure of the human telomeric g-quadruplexes and exert anti-tumor activity (Bessi et al., 2012). Su et al. found that berberine bound to vasodilator-stimulated phosphoproteins, induced changes in their secondary structure and inhibited actin polymerization (Su et al., 2016). Yi et al. reported that berberine directly bound to actin and inhibited the migration of mouse mononuclear macrophage leukemia cells and mouse embryonic fibroblasts (Yi et al., 2017). However, the direct binding targets

[1]State Key Laboratory of Coordination Chemistry, School of Chemistry and Chemical Engineering, Collaborative Innovation Center of Advanced Microstructures, Nanjing University, Nanjing 210023, P.R. China

[2]Department of Pharmacology, Affiliated Hospital of Nanjing University of Chinese Medicine, Nanjing 210029, P. R. China

[3]Lead contact

*Correspondence: gengzr@nju.edu.cn (Z.-R.G.), majing@nju.edu.cn (J.M.), wangzl@nju.edu.cn (Z.-L.W.)

https://doi.org/10.1016/j.isci.2022.104773

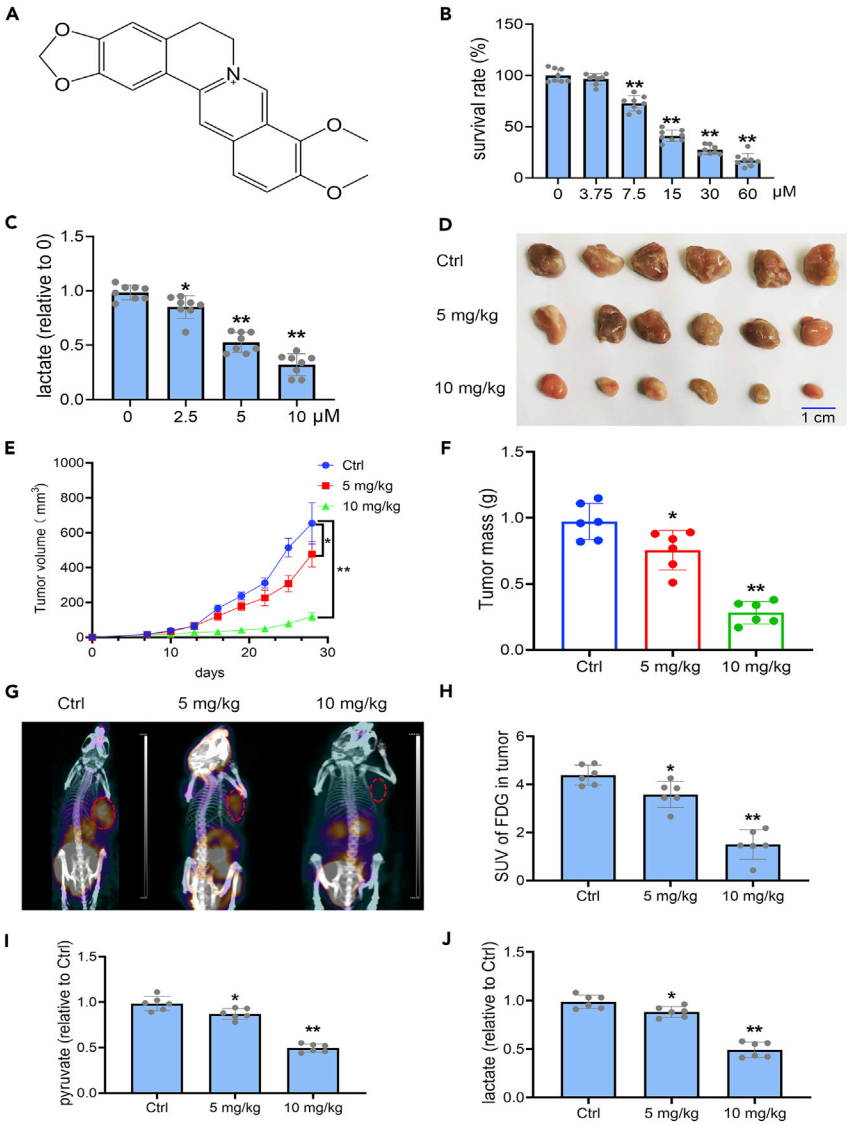

Figure 1. Berberine inhibits colorectal cancer with improved metabolism

(A) Chemical structure of Berberine.

(B) Berberine inhibits the proliferation of HT29 cells.

(C) Berberine inhibits lactate production in HT29 cells.

(D–J) Berberine inhibits tumor growth in HT29 cell-bearing mice intraperitoneally injected with berberine (5 or 10 mg/kg body weight) for 28 days, including (D) Tumor pictures; (E) Tumor volume; (F) Tumor weight; (G) Representative FDG PET/CT images; (H) SUV of FDG in tumor indicating glucose uptake; (I) Tumor pyruvate production. (J) Tumor lactate production. The data are shown as the mean ± SD of three independent experiments. Statistics differences were analyzed by one-way ANOVA followed by Dunnett's post-hoc test. *$p < 0.05$, **$p < 0.01$.

investigated in previous studies are not sufficient to elucidate the role of berberine in improving the metabolic reprogramming of colorectal cancer.

As an important technical tool in chemical biology research, chemical proteomics has become a new model for studying the mechanism of action of natural drug components, which is useful for facilitating the development of natural drug chemistry into new drugs. The general process of chemical proteomics involves the incubation of chemical probes or compound matrices with protein extracts, protein separations using affinity chromatography, identification by highly sensitive mass spectrometry (MS), followed by bioinformatics analysis. When a drug molecule is found to have a therapeutic effect but it is not clear which protein it

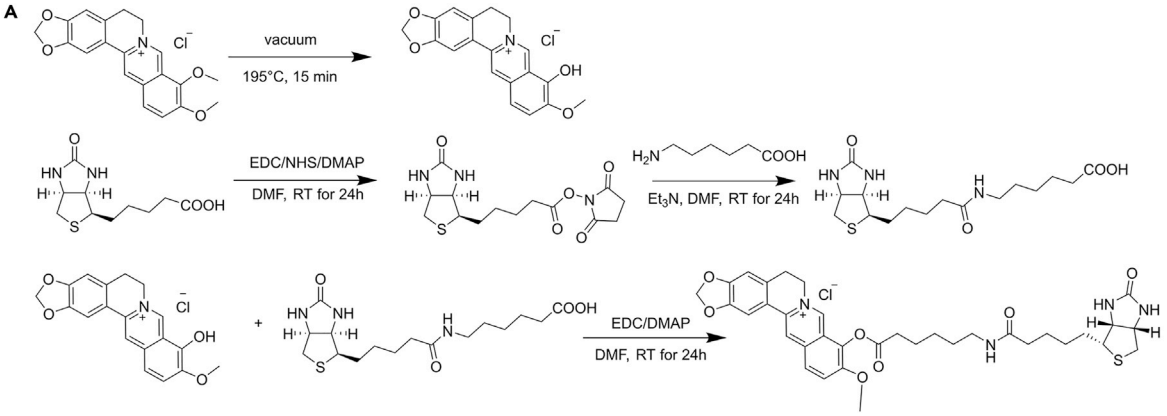
A
vacuum
195°C, 15 min
EDC/NHS/DMAP
DMF, RT for 24h
Et3N, DMF, RT for 24h
EDC/DMAP
DMF, RT for 24h

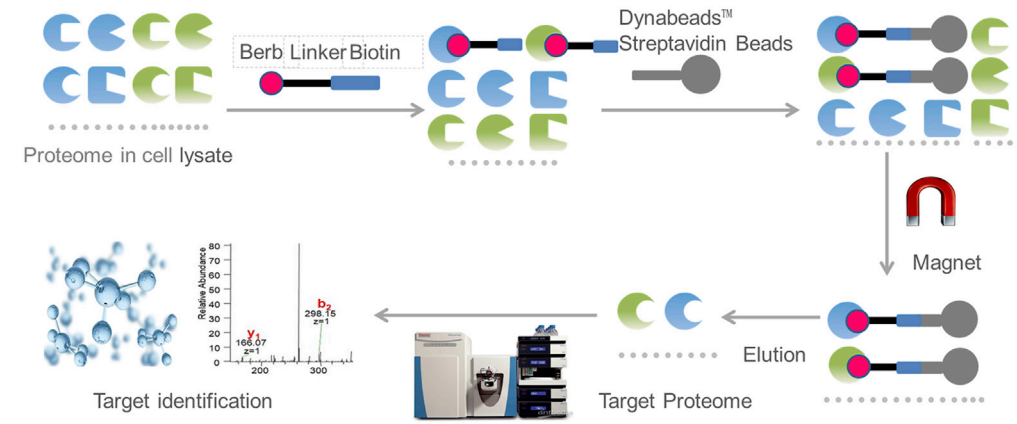
B
Berb Linker Biotin
Dynabeads™
Streptavidin Beads
Proteome in cell lysate
Magnet
Elution
Target Proteome
Target identification

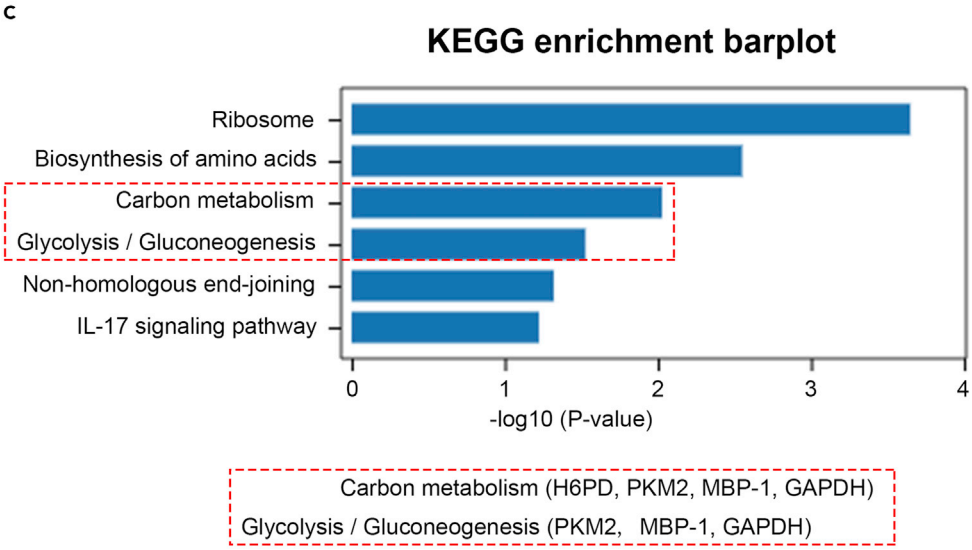
C
KEGG enrichment barplot
Ribosome
Biosynthesis of amino acids
Carbon metabolism
Glycolysis / Gluconeogenesis
Non-homologous end-joining
IL-17 signaling pathway
0
1
2
3
4
-log10 (P-value)
Carbon metabolism (H6PD, PKM2, MBP-1, GAPDH)
Glycolysis / Gluconeogenesis (PKM2, MBP-1, GAPDH)

Figure 2. Chemoproteomic identification of direct binding target proteins of berberine in colorectal cancer cells
(A) Synthesis pathway diagram of biotinylated berberine.
(B) Flow chart of chemical proteomics study.
(C) Top six of pathway enrichment through bioinformatics analyses. The data are shown from three independent experiments.

acts on, chemical proteomics is used to "catch" the target protein out of thousands of proteins (Chen et al., 2020a).

PKM2 plays an important role in tumor and inflammation-related diseases (Li et al., 2018). In this study, a chemical proteomics approach was used to identify PKM2, the direct target protein of berberine in colorectal cancer cells. Combining computational chemistry and molecular biological technique, it was revealed that the key sites of PKM2 binding by berberine were I119 and F244. The binding of berberine to PKM2 resulted in an increase in the ubiquitination and degradation of PKM2. Moreover, berberine was shown to inhibit the reprogramming of glucose metabolism and the phosphorylation of STAT3, downregulate the expression of Bcl-2 and Cyclin D1 genes, inhibit cell proliferation and promote apoptosis, ultimately inhibiting the progression of colorectal cancer.

RESULTS

Berberine inhibited the progression of colorectal cancer and improved the metabolic function of colorectal cancer cells

In vitro, berberine inhibited the proliferation of colorectal cancer cells HT29 and HCT116 with EC_{50} of 4.62 μM and 9.39 μM, respectively (Figures 1B and S1A). Further assays showed that berberine inhibited lactate production (Figure 1C), promoted apoptosis (Figures S1B and S1C), and blocked the cell cycle in the G0-G1 phase (Figures S2A and S2B). *In vivo* experiments showed that tumor growth was inhibited in HT29 cell-bearing mice injected intraperitoneally with berberine (5 or 10 mg/kg body weight) (Figures 1D-1F). 2-Deoxy-2-[F-18]fluoro-D-glucose positron emission tomography/computed tomography (FDG PET/CT) is used for the tumor diagnosis and evaluation of glucose metabolism (Facchin et al., 2020). The results showed a significant reduction in tumor size and standard uptake value (SUV) of FDG in HT29 cell-bearing mice (Figures 1G and 1H). Pyruvate and lactate production were also inhibited (Figures 1I and 1J). These *in vitro* and *in vivo* observations indicated that berberine inhibited the progression of colorectal cancer and improved the metabolic function of colorectal cancer cells.

Chemical proteomics identified the direct binding protein of berberine

As the direct binding target proteins of berberine involved in the metabolic reprogramming of colorectal cancer cells and the progression of colorectal cancer have not been reported, the chemical proteomic technique was used to explore the direct binding target proteins of berberine to inhibit the metabolic reprogramming of colorectal cancer cells. Firstly, biotinylated berberine (biotin-aminocaproic acid-berberine ester) was synthesized, and the synthesis flow chart is shown in Figure 2A.

Biotinylated berberine was characterized by MS (Figure S3), hydrogen spectroscopy (Figure S4), and carbon spectroscopy (Figure S5). The structural information of biotinylated berberine was obtained by NMR and mass spectra:^{1}H NMR (400 MHz, DMSO-d6) δ 10.02 (s, 1H), 9.06 (s, 1H), 8.28 (d, *J* = 9.4, 1H), 8.21 (d, *J* = 9.2, 1H), 7.93 (t, *J* = 5.6, 1H), 7.81 (s, 1H), 7.09 (s, 1H), 6.43 (s, 1H), 6.38 (s, 1H), 6.17 (s, 2H), 4.98 (t, *J* = 6.1, 2H), 4.29 (dd, *J* = 7.6, 5.1, 1H), 4.12 (m, 1H), 4.03 (s, 3H), 3.22 (t, *J* = 5.9, 2H), 3.08 (dq, *J* = 12.3, 6.3, 3H), 2.88 (dd, *J* = 8.8, 5.8, 2H), 2.80 (dd, *J* = 12.4, 5.1, 1H), 2.57 (d, *J* = 12.4, 1H), 2.07 (t, *J* = 7.3, 2H), 1.74 (t, *J* = 7.2, 2H), and 1.65–1.2 (m, 12H). ^{13}C NMR (400 MHz, DMSO-d6) δ 171.96, 170.66, 162.75, 150.39, 149.98, 147.72, 144.49, 138.08, 133.59, 132.93, 130.87, 126.70, 125.87, 121.19, 120.62, 120.39, 108.45, 105.57, 102.15, 61.07, 59.23, 57.23, 55.47, 55.23, 39.86, 38.26, 35.25, 33.19, 28.92, 28.26, 28.08, 26.20, 25.79, 25.38, and 23.99. ESI-MS (methanol), *m/z* calcd for ($C_{35}H_{41}N_4O_7S^+Cl^-$, $[M-Cl]^+$), 661.27; found, 661.42.

The anti-tumor activity of biotinylated berberine was examined as part of the chemoproteomics study and biotinylated berberine showed an inhibitory effect on colorectal cancer cell HT29 with EC_{50} of 3.47 μM which was similar to berberine (Figure S6), supporting biotinylated berberine as a chemoproteomics tool.

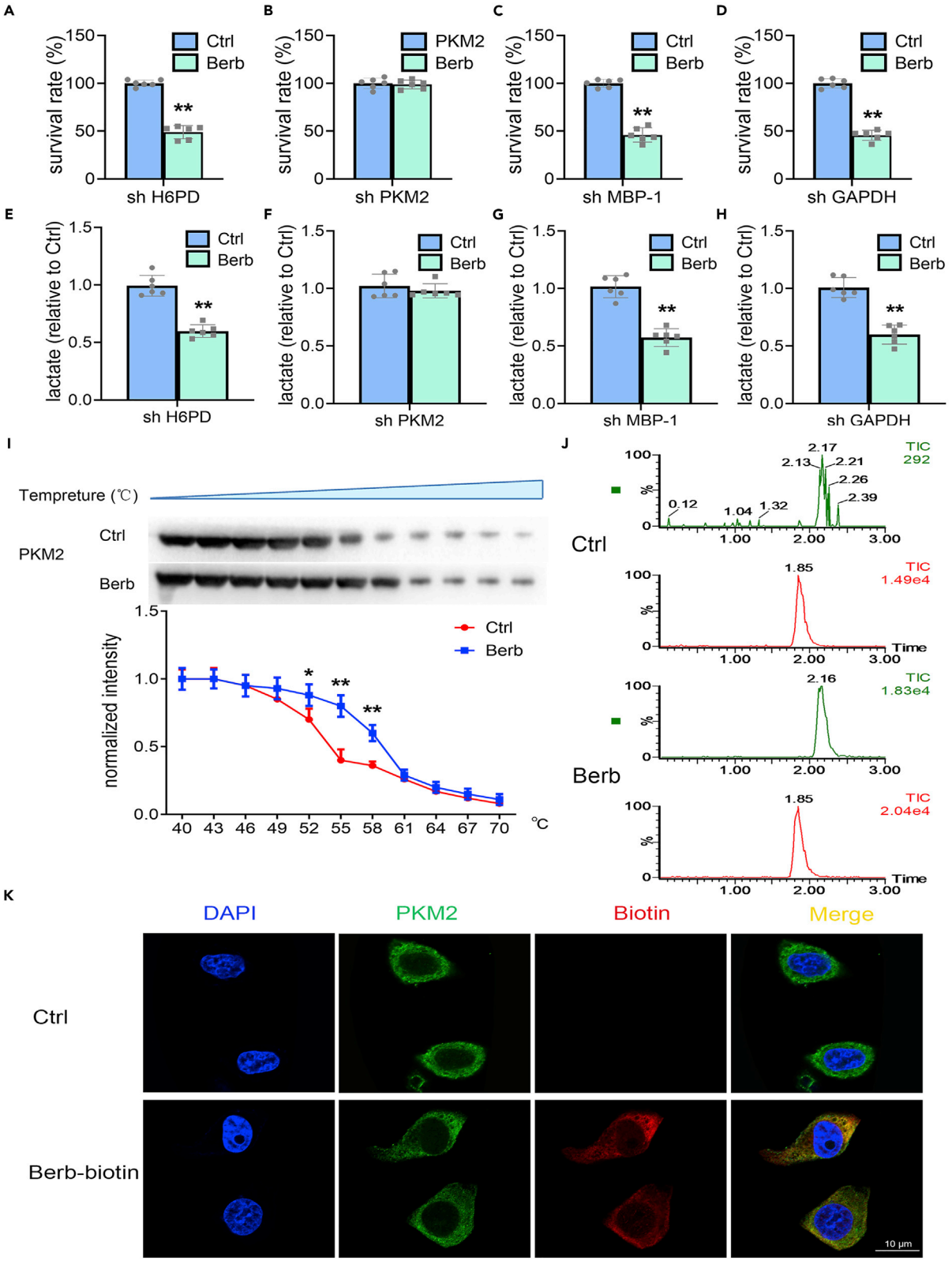
A
B
C
D
survival rate (%)
Ctrl
Berb
PKM2
**
sh H6PD
sh PKM2
sh MBP-1
sh GAPDH
E
F
G
H
lactate (relative to Ctrl)
I
Tempreture (℃)
PKM2
Ctrl
Berb
normalized intensity
*
**
℃
J
TIC
292
1.49e4
1.83e4
2.04e4
Time
K
DAPI
PKM2
Biotin
Merge
Berb-biotin
10 μm

Figure 3. Berberine interacts directly with PKM2

(A–D) Effect of berberine on the proliferation of HT29 cells after knockdown of metabolic pathway proteins H6PD, PKM2, MBP-1, or GAPDH.

(E–H) The effect of berberine on the lactate production of HT29 cells after knockdown of metabolic pathway proteins H6PD, PKM2, MBP-1, or GAPDH.

(I) Thermal migration method to detect the interaction of berberine with PKM2 in HT29 cell (n = 3).

(J) Determination of berberine bound with PKM2 of HT29 cells co-incubated with vehicle or berberine (5 μM) for 30 min.

(K) Co-localization of PKM2 and biotinylated berberine was detected by Immunofluorescence after HT29 cells were incubated with biotinylated berberine for 30 min. Scale bar, 10 μm. The data are shown as the mean ± SD of three independent experiments. Statistics differences were analyzed by one-way ANOVA followed by Dunnett's post-hoc test. *$p < 0.05$, **$p < 0.01$.

Based on the chemoproteomics study outlined in the flow chart (Figures 2B), 52 possible direct binding target proteins were detected (Table S1). Through bioinformatics analysis, four proteins were identified to be associated with metabolic reprogramming, namely H6PD, PKM2, MBP-1, and GAPDH (Figure 2C).

Berberine inhibited colorectal cancer progression by direct targeting PKM2

Berberine inhibited significantly the proliferation and lactate production of colorectal cancer cells when H6PD, MBP-1, or GAPDH was knocked down (Figures 3A, 3C, 3D, 3E, 3G, and 3H). The inhibitory effect of berberine on the proliferation and lactate production of colorectal cancer cells was found to be significantly attenuated or disappeared when PKM2 was knocked down (Figures 3B and 3F). These results indicate that berberine can directly bind PKM2 to produce pharmacological effects. MS/MS spectra shown in Figures S7 and S8 demonstrated the trypsin-digested peptide fragments belong to PKM2 confirmed by further library search, which indicates that berberine binds directly to PKM2 in HT29 cells.

Thermal transfer assay is a biophysical technique for the direct study of ligands that bind proteins in cells and tissues. The cellular thermal migration analysis further confirmed the presence of direct binding of berberine to PKM2 in HT29 cells (Figure 3I).

The immunoprecipitated PKM2 was further analyzed by liquid chromatography-mass spectrometry (LC-MS) to determine the binding of berberine to PKM2 based on our previous detection methods (Dai et al., 2018a). The chromatograms of the control and berberine groups are shown in Figure 3J. The secondary mass spectra of berberine are shown in Figure S9A, the chromatogram of the blank sample is shown in Figure S9B, and the chromatogram of the berberine standard is shown in Figure S9C. (Green is the berberine detection channel and red is the internal standard detection channel. According to the guidelines for the bioanalytical method recommended by US Food and Drug Administration (US Food and Drug Administration, 2013), the interference was considered acceptable if the peak area counts of analytes and IS were not more than 20% for analytes, and 5% for IS, compared to the area counts in the berberine sample. For this detection, the chromatogram of the blank sample and control group exhibit insignificant interference which was far less than 20%. Therefore, the interference peak did not affect the accuracy and precision).

Immunofluorescence detection showed the co-localization of biotinylated berberine (green) with PKM2 (red) expression (Figure 3K).

Mechanism of interaction of berberine with PKM2 in inhibiting colorectal cancer

HT29 cells were used for the *in vitro* detection of the activity, protein, and gene levels of PKM2 in the presence of berberine. Berberine inhibited PKM2 activity (Figure S9D) and its protein level (Figure 4A), but did not affect its mRNA (Figure 4C). The protein (Figure 4A) and mRNA (Figure 4D) levels were unaffected for PKM1.

Considering that berberine directly down-regulated the expression of PKM2 protein, we speculated that berberine affected the stability of PKM2 through the level of post-translational modification of the protein. We examined the effect of berberine on PKM2 ubiquitination. The low levels of PKM2 ubiquitination were detected in the blank control group, indicating a systemic equilibrium process between the synthesis and ubiquitination degradation of PKM2 in tumor cells. In contrast, berberine increased ubiquitination (Figure 4B).

In contrast to PKM2 inhibition, berberine showed no effect on the expression of ubiquitin ligase Stub1 (specific ubiquitin ligase for the degradation of PKM2 (Shang et al., 2017) by the immunoconfocal technique

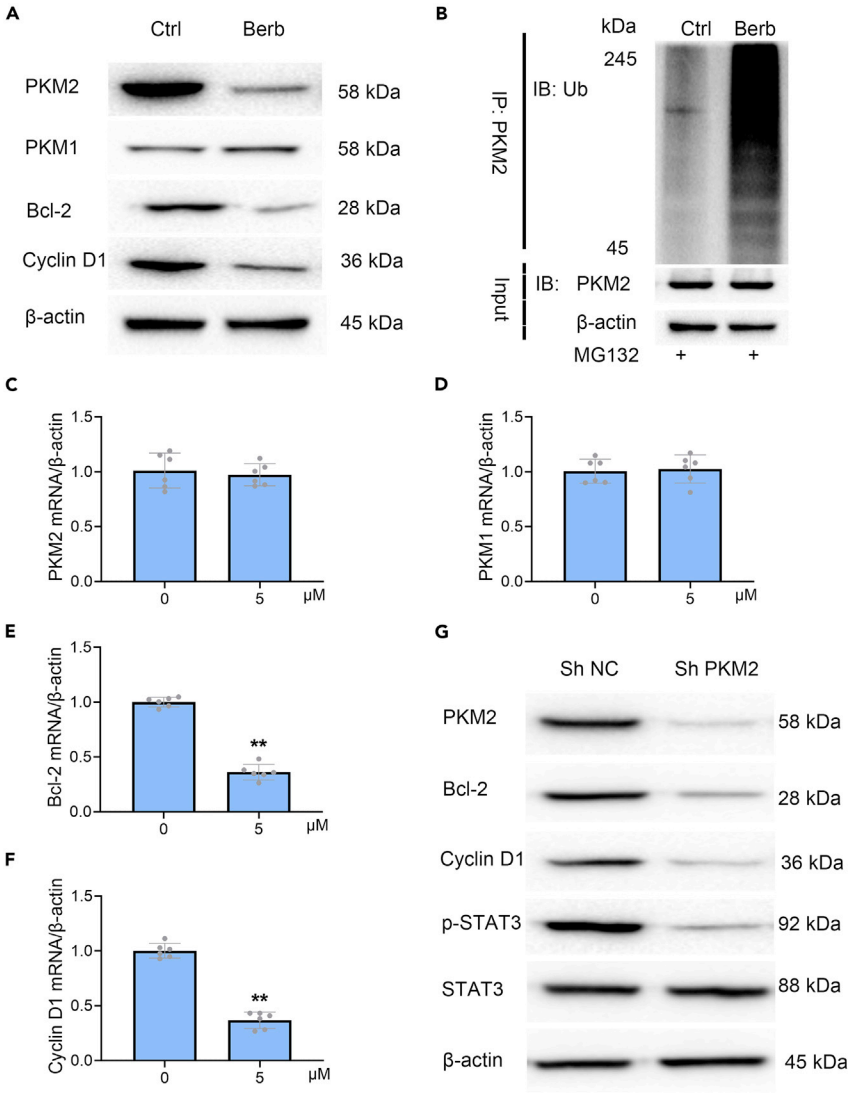

Figure 4. Direct binding of berberine to PKM2 promotes ubiquitination to inhibit the pathway in colorectal cancer

(A) The effect of berberine on PKM2, PKM1, Bcl-2, Cyclin D1 expression in HT29 cells was studied using Western blot analysis.

(B) Berberine promotes PKM2 ubiquitination.

(C) PKM2 mRNA levels (n = 6).

(D) PKM1 mRNA levels (n = 6).

(E) Bcl-2 mRNA levels (n = 6).

(F) Cyclin D1 mRNA levels (n = 6).

(G) The effect of Sh PKM2 on Bcl-2, Cyclin D1, and STAT3 phosphorylation in HT29 cells was studied using Western blot analysis. The data are shown as the mean ± SD of three independent experiments. Statistics differences were analyzed by unpaired t test. *$p < 0.05$, **$p < 0.01$.

(Figure S9E), suggesting that berberine may promote the ubiquitination of PKM2 by directly targeting PKM2 and changing its spatial structure.

In addition, berberine caused decreases in protein (Figure 4A) and mRNA (Figures 4E and 4F) levels of Bcl-2 and Cyclin D1, accompanied by an increase in apoptosis, and cell-cycle arrest at the G0-G1 phase and inhibition of proliferation.

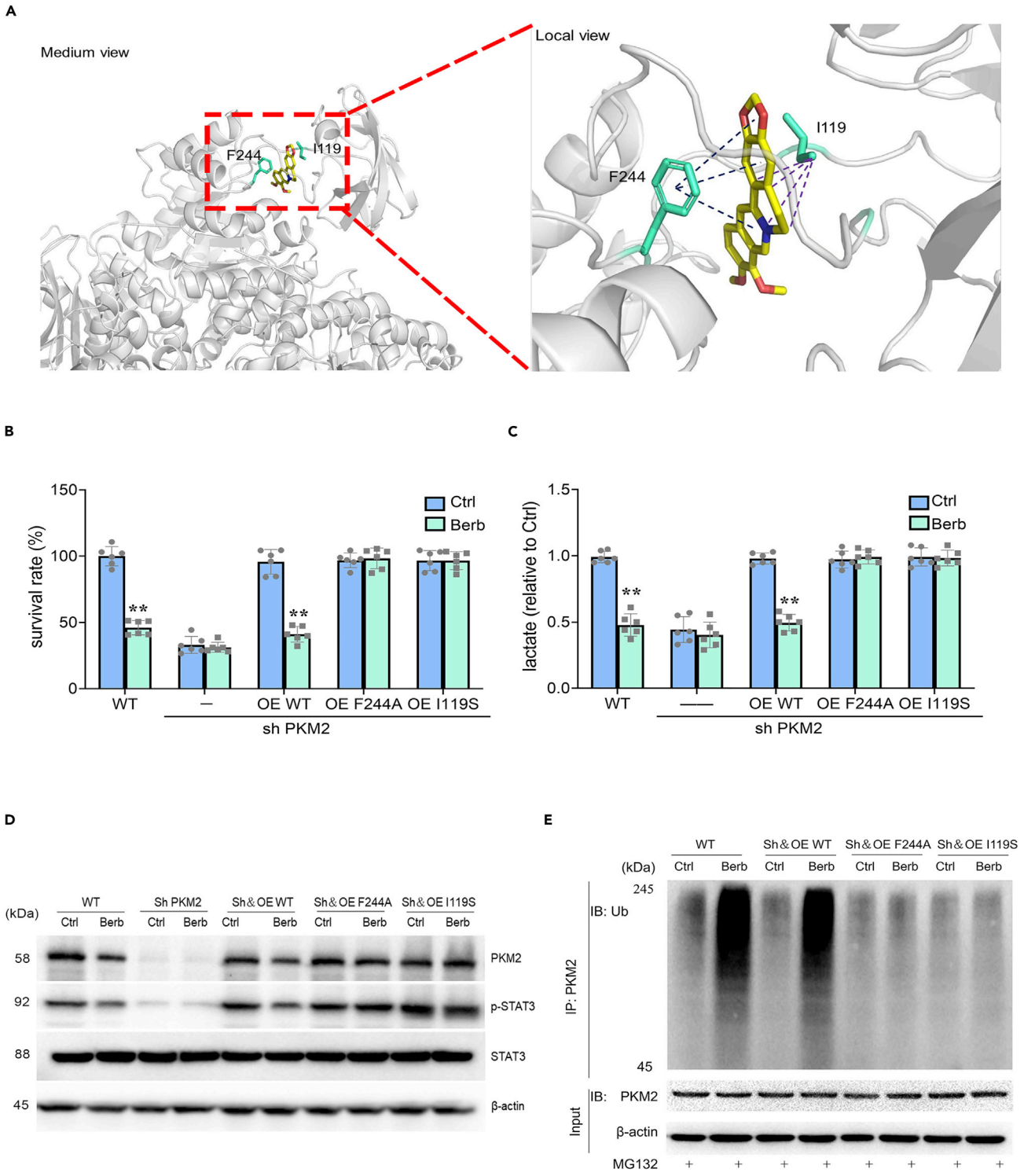

Figure 5. Structural model study of berberine-PKM2 binding

(A) Spatial conformation of berberine-PKM2 binding.

(B) Effect of berberine on cell proliferation after the knockdown or mutation of the PKM2 amino acid site (n = 6).

Figure 5. *Continued*

(C) Effect of berberine on lactate production after the knockdown or mutation of the PKM2 amino acid site (n = 6).

(D) Effect of berberine on the expression of PKM2 and p-STAT3 in HT29 cells after the knockdown or mutation of the PKM2 amino acid site.

(E) Effect of berberine on the ubiquitination of PKM2 after the knockdown or mutation of the PKM2 amino acid site. The data are shown as the mean ± SD of three independent experiments. Statistics differences were analyzed by unpaired t test. *p < 0.05, **p < 0.01.

PKM2 is not only a glycolytic enzyme but also an active protein kinase that phosphorylates oncogene signal transduction and transcriptional activator 3 (STAT3) at the Y705 site and promotes cancer cell proliferation (Gao et al., 2012; Christofk et al., 2008). PKM2 gene silencing inhibited the phosphorylation of STAT3, which in turn inhibited the expression of downstream factors Bcl-2 and Cyclin D1 (Figure 4G).

Structural modeling and simulation of berberine-PKM2 binding

Based on the sequence of the protein (3gr4) given by RCSB PDB (http://www.rcsb.org/), the structure of 3gr4 was developed by homology modeling with 4jpg as a template on the SWISS-MODEL server (Waterhouse et al., 2018). The initial coordinate of berberine was retrieved from the TCMSP database (Ru et al., 2014) and was optimized by Avogadro 1.2.0 (http://avogadro.cc/).

Both rigid and flexible dockings were carried out on 3gr4 using AutoDock Vina software with a default configuration setting (https://vina.scripps.edu/tutorial/) (Trott and Olson, 2010). The flexible docking studies show that berberine is docked to the residue N210 of 3gr4 in all the 20 best-scoring binding modes with binding affinity from −6.7 to −8.0 kcal/mol (Table S2). The structure of the binding mode was selected as the initial complex for MD simulations (Figure S10A).

Distance analysis along the 80ns MD trajectory was carried out to visualize the time evolution of the relevant distance between the berberine and its nearest amino acids with both the ff99sb and ff14sb force field. An emphasis was laid on protein residues that are within 4 Å of the berberine at the start or end of the trajectory. The evolution of the distances between I119, V209, N210, V216, F244 with respect to berberine molecule with time was recorded separately. V209, N210, and V216 appeared to move away, and fluctuations around 4 Å of F244 and I119 indicate their stable interactions with berberine molecule (Figures S10B and S10C). The extension of MD duration just caused slight changes in both the RMSD (Figure S10D) and potential energies (Figure S10E).

The inner oxygen ring and N atomic ring on the berberine molecule interacted with F244 amino acid residue via π-π interaction and with the I119 amino acid residue of PKM2 via hydrophobic interaction, forming an overall structure similar to a sandwich (Figure 5A). A 2D format of docking interactions predicted by MD simulations was presented in SI (Figure S10F) (Laskowski and Swindells, 2011).

The binding free energy calculation with Molecular Mechanics/Poisson-Boltzmann Area (MM/PBSA) based on amino acid site-mutation revealed that the "sandwich" structure was disrupted by mutating F244 (phenylalanine) to alanine (F244A) or I119 (isoleucine) to serine (I119S) (Figure S11A, S11B, and Table S3). These results suggest that F244 and I119 may be the key amino acid sites of interaction between berberine and PKM2.

The knockdown and overexpression experiments were used to verify the role of PKM2. As expected, the inhibitory effect of berberine on the survival of HT29 cells disappeared after the knockdown of PKM2. However, the effect was restored after the overexpression of the homologous PKM2. Even after overexpression of the two PKM2 mutants F244A or I119S in HT29 cells, respectively, the inhibitory effects of berberine on the survival of colorectal cancer cells were not observed (Figure 5B). The same trends were seen for lactate production (Figure 5C).

In addition, PKM2 knockdown significantly decreased PKM2 expression and STAT3 phosphorylation, while both homologous PKM2 overexpression and overexpression of PKM2 with mutant F244A or I119S significantly increased STAT3 phosphorylation level. Berberine inhibited PKM2 expression and STAT3 phosphorylation in the wild-type and homologous mutant strains of HT29 cells, but not in the two strains with mutant F244A or I119S (Figure 5D).

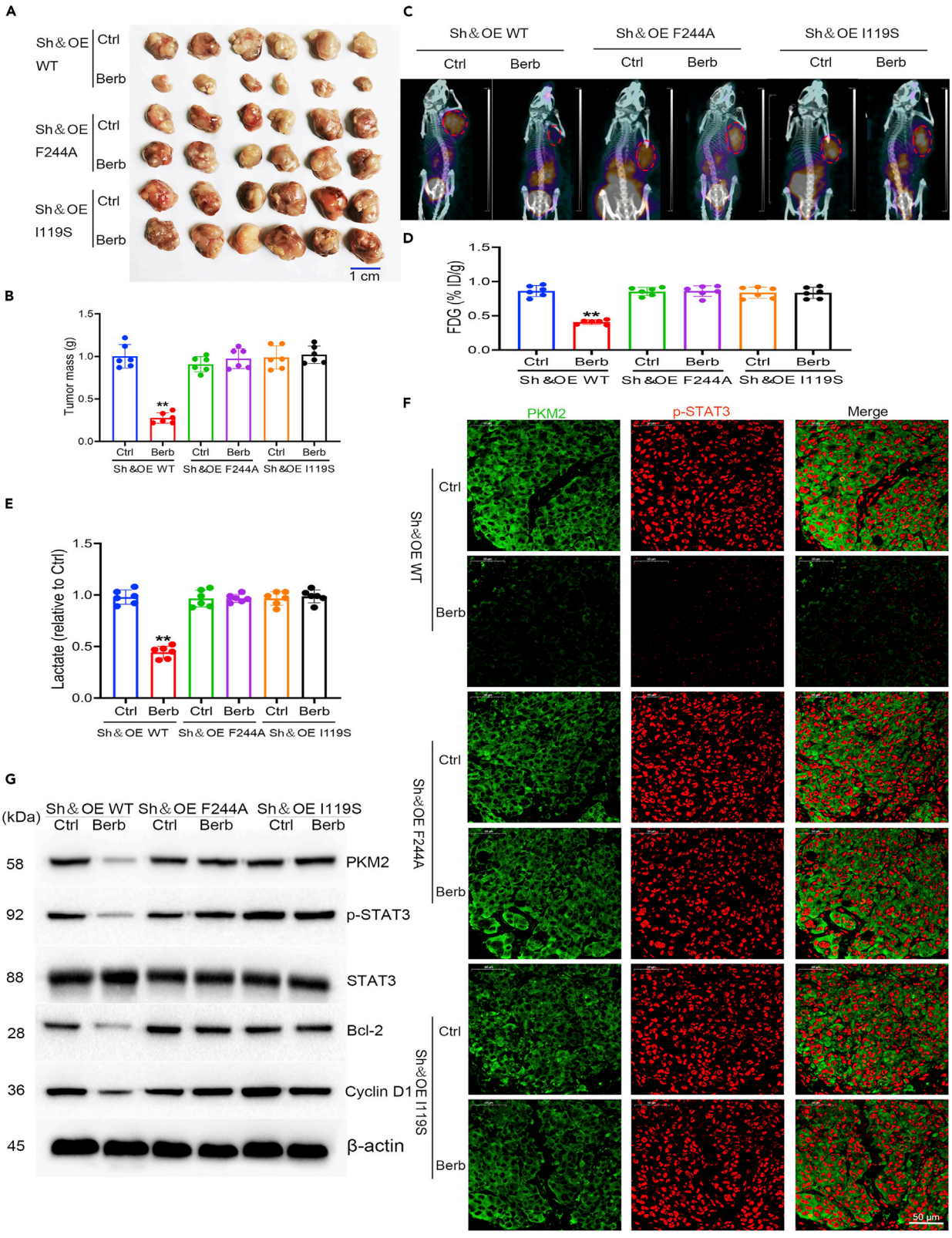
A
Sh&OE WT
Ctrl
Berb
Sh&OE F244A
Ctrl
Berb
Sh&OE I119S
Ctrl
Berb
1 cm
B
Tumor mass (g)
1.5
1.0
0.5
0.0
**
Ctrl
Berb
Ctrl
Berb
Ctrl
Berb
Sh &OE WT
Sh &OE F244A
Sh &OE I119S
C
Sh&OE WT
Sh&OE F244A
Sh&OE I119S
Ctrl
Berb
Ctrl
Berb
Ctrl
Berb
D
FDG (% ID/g)
1.5
1.0
0.5
0.0
**
Ctrl
Berb
Ctrl
Berb
Ctrl
Berb
Sh &OE WT
Sh &OE F244A
Sh &OE I119S
E
Lactate (relative to Ctrl)
1.5
1.0
0.5
0.0
**
Ctrl
Berb
Ctrl
Berb
Ctrl
Berb
Sh&OE WT
Sh&OE F244A
Sh&OE I119S
F
PKM2
p-STAT3
Merge
Sh&OE WT
Ctrl
Berb
Sh&OE F244A
Ctrl
Berb
Sh&OE I119S
Ctrl
Berb
50 μm
G
(kDa)
Sh&OE WT
Ctrl
Berb
Sh&OE F244A
Ctrl
Berb
Sh&OE I119S
Ctrl
Berb
58
PKM2
92
p-STAT3
88
STAT3
28
Bcl-2
36
Cyclin D1
45
β-actin

Figure 6. CDX models to validate berberine-PKM2 binding site inhibition in colorectal cancer cell HT29

Nude mice were inoculated with Sh/OE PKM2 (homologous mutation) HT29 cells, Sh/OE PKM2 (F244A) HT29 cells, or Sh/OE PKM2 (I199S) HT29 cells to construct xenograft mouse models and intraperitoneally injected with vehicle or berberine (10 mg/kg body weight) for 28 days.

(A) Tumor pictures. Scale bar, 1 cm.

(B) Tumor weight (n = 6).

(C) Representative FDG PET/CT images.

(D) SUV of FDG in tumor indicating glucose uptake (n = 6).

(E) Lactate production (n = 6).

(F) PKM2 and p-STAT3 expression.

(G) Representative Western blot analysis of PKM2 and downstream proteins after amino acid site mutation. Scale bar, 50 μm. The data are shown as the mean ± SD of three independent experiments. Statistics differences were analyzed by one-way ANOVA followed by Dunnett's post-hoc test. *$p < 0.05$, **$p < 0.01$.

Similar results were seen *in vitro* PKM2 ubiquitination assay after immunoprecipitation. An increase in PKM2 ubiquitination was detected in the HT29 cell line expressing wild-type and homologous mutational PKM2 not in the cell lines with mutant F244A or I119S under treatment with berberine (Figure 5E).

Cell-derived xenograft models confirmed that berberine directly bound to I119 and F244 of PKM2

Nude mice were inoculated with Sh/OE PKM2 (homologous mutation, similar to WT, HWT) HT29 cells, Sh/OE PKM2 (F244A) HT29 cells, or Sh/OE PKM2 (I199S) HT29 cells to construct xenograft mouse models and treated with berberine (10 mg/kg) intraperitoneally. Berberine decreased the tumor volumes in nude mice transplanted with HWT cells, compared with no changes in the tumor volumes and weights in nude mice transplanted with F244A and I199S mutant cells (Figures 6A and 6B). The same trend was seen for PET/CT results (Figures 6C and 6D).

Berberine inhibited the proliferation index (Ki67 expression) and promoted the apoptotic index (Tunel) of HWT cells, and no changes were observed in F244A or I199S mutant cells (Figures S12A and S12B).

Berberine inhibited lactate production, glucose uptake, pyruvate production, and PKM2 activity in HWT tumor tissues, but no apparent effects were observed in both F244A mutant cells and I199S mutant tumor tissues (Figures 6E, 6D, S14D, and S14E).

Berberine inhibited the co-expression of PKM2 with p-STAT3 in HWT HT29 tumor tissues not in F244A or I199S mutant tumor tissues by immunofluorescence detection Figure 6F).

Heat migration analysis showed the binding of PKM2 with berberine in HWT cells (Figure S13A), without apparent interactions seen in both F244A and I199S mutant cells (Figure S13C and S13E). The co-localization study of PKM2 and biotinylated berberine showed that the biotinylated berberine content in the PKM2-expressing region was higher in HWT cells Figure S13B) compared with a significant reduction in F244A or I199S mutant cells (Figures S13D and S1F). MS combined with immunoprecipitation showed high content of berberine in PKM2 of HWT HT29 cells (Figure S14A) and no berberine was detected in PKM2 of F244A or I199S mutant cells (Figures S14B and S14C).

Western blotting showed that PKM2, p-STAT3, Bcl-2, and Cyclin D1 were significantly decreased in HWT HT29 cells after berberine intervention, but no change was apparent in F244A or I199S mutant cells (Figure 6G).

Patient-derived xenograft models confirmed that berberine inhibited colorectal cancer progression by binding to PKM2 and promoting its ubiquitination

Patient-derived xenograft (PDX) models were established using intestinal cancer tissues from three different patients, and berberine was administered intraperitoneally. The colorectal cancer tumor growth was inhibited by berberine, as measured by tumor volumes and weight changes shown in Figures 7A and 7B. The FDG PET/CT results showed a significant reduction in tumor size and glucose uptake (Figures 7C and 7D). Compared with controls, the PKM2 ubiquitination was increased (Figure 7E) in berberine-treated groups, accompanied by decreased lactate production (Figure 7F), pyruvate production and PKM2 activity (Figures S15A and S15B), proliferation of colorectal cancer tissues (Figure S15C) and

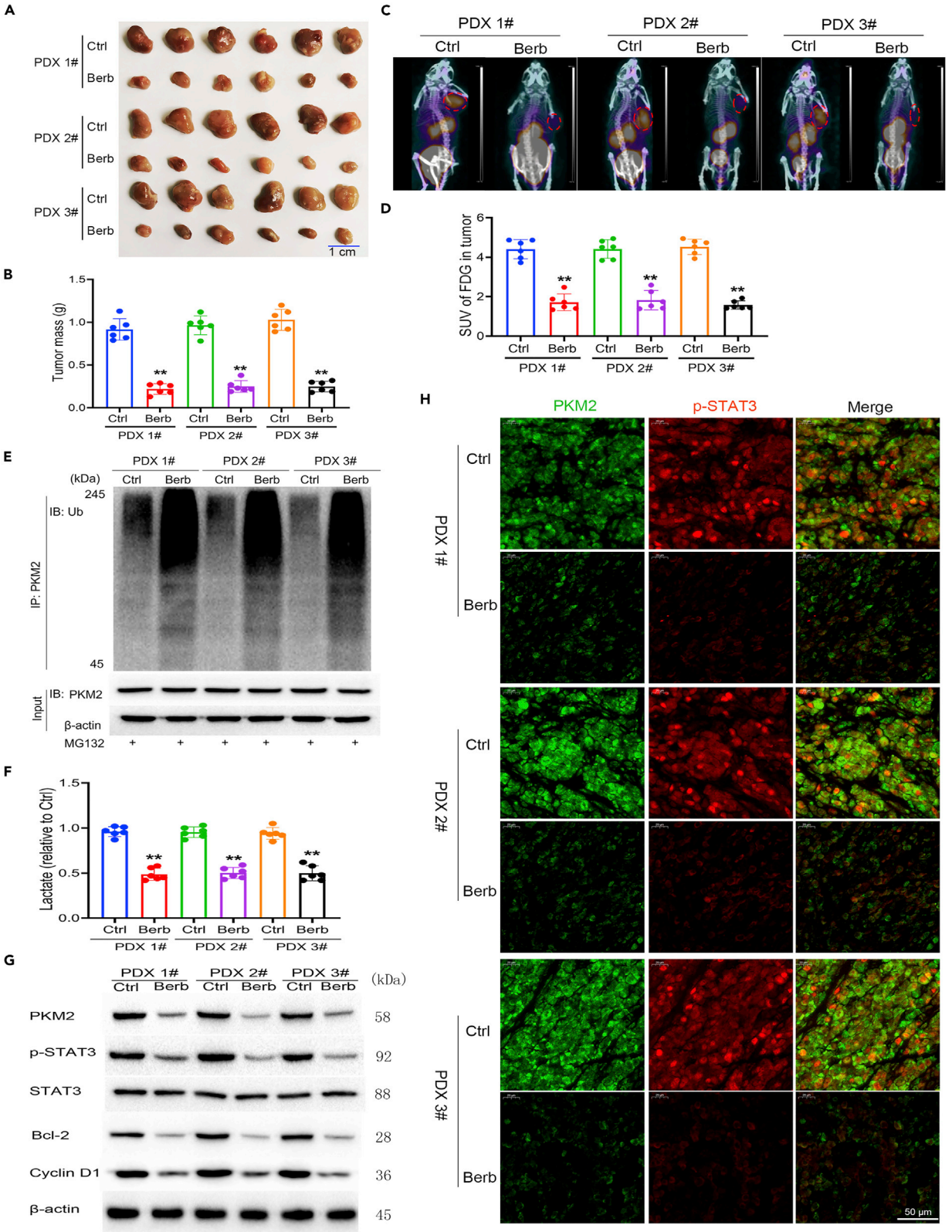
A
PDX 1#
Ctrl
Berb
PDX 2#
Ctrl
Berb
PDX 3#
Ctrl
Berb
1 cm
B
Tumor mass (g)
1.5
1.0
0.5
0.0
**
Ctrl
Berb
PDX 1#
PDX 2#
PDX 3#
C
PDX 1#
PDX 2#
PDX 3#
Ctrl
Berb
D
SUV of FDG in tumor
6
4
2
0
E
(kDa)
245
45
IP: PKM2
IB: Ub
Input
IB: PKM2
β-actin
MG132
F
Lactate (relative to Ctrl)
G
PKM2
p-STAT3
STAT3
Bcl-2
Cyclin D1
β-actin
58
92
88
28
36
45
H
PKM2
p-STAT3
Merge
PDX 1#
PDX 2#
PDX 3#
Ctrl
Berb
50 μm

Figure 7. PDX models confirm that berberine promotes PKM2 ubiquitination to inhibit colorectal cancer

PDX models were established using intestinal cancer tissues from three different patients and intraperitoneally injected with vehicle or berberine (10 mg/kg body weight) for 28 days.

(A) Tumor pictures. Scale bar, 1 cm.

(B) Tumor weight (n = 6).

(C) Representative FDG PET/CT images.

(D) SUV of FDG in tumor indicating glucose uptake (n = 6).

(E) PKM2 ubiquitination.

(F) Lactate Production (n = 6).

(G) Representative Western blot analysis of PKM2 and downstream proteins.

(H) PKM2 and p-STAT3 expression. Scale bar, 50 μm. The data are shown as the mean ± SD of three independent experiments. Statistics differences were analyzed by one-way ANOVA followed by Dunnett's post-hoc test. *$p < 0.05$, **$p < 0.01$.

increased apoptosis of colorectal cancer cells (Figure S15D), as well as inhibited co-expression of PKM2 and P-STAT3 (Figure 7H) and phosphorylation of STAT3, and down-regulated expressions of Bcl-2 and Cyclin D1 (Figure 7G).

DISCUSSION

Berberine, a bioactive ingredient of *Rhizoma coptidis* and *Phellodendron phellodendron*, has been reported to improve the metabolism of colorectal cancer cells, promote cell apoptosis and inhibit cell proliferation (Mao et al., 2018; Wu et al., 2018; Li et al., 2015) and inhibit tumor progression in other types of cancer by modulating the Warburg effect (Li et al., 2021b). However, the target proteins of berberine have not been reported. Precise identification of molecular targets is essential for the development of natural active drugs for the treatment of colorectal cancer and can help guide the structural optimization of natural components (Spradlin et al., 2019). Chemical proteomics has become a valuable tool for discovering protein targets of natural product components with specific biological activities (Dai et al., 2018b; Chen et al., 2019, 2021; Kotake et al., 2007; Abegg et al., 2015). It will provide important clues to guide the functional elucidation of their mechanisms of action and open new windows for drug development. In our studies, we used a chemical proteomic strategy with biotin-avidin system to identify protein targets of berberine and confirmed that PKM2 is a direct target of berberine, which was further identified by the gene knockout technology.

PKM2 gene silencing inhibits cancer cell proliferation and promotes apoptosis (Goldberg and Sharp, 2012; Wong et al., 2015), but the complete deletion of PKM2 does not inhibit tumor growth in mouse models (Israelsen et al., 2013; Dayton et al., 2016). In addition, protein kinase activity was not detected from the purified PKM2 protein [Hosios et al., 2015], suggesting that the role of PKM2 *in vivo* is complex. In the thermal migration assay, a biophysical technique that allows the direct study of ligands binding to proteins in cells and tissues (Molina et al., 2013; Dai et al., 2019), the interaction between berberine and PKM2 was observed, as reflected by a slower decreasing trend in PKM2 expression in berberine group. Laser confocal microscopy observed that biotinylated berberine was significantly increased in the PKM2-expressing region. In addition, bound berberine was detected in PKM2 using immunoprecipitation PKM2 binding MS. PKM1 has different spatial conformation and function from PKM2 owing to 23 amino acids at C-terminus. Based on our chemical proteomics, berberine selectively and directly targeted PKM2 rather than PKM1, consistent with the strong inhibitory effect on PKM2, not PKM1 reported in the literature (Yang et al., 2014).

The high expression of PKM2 promotes the malignant process of colorectal cancer. We found that in colorectal cancer cells, proliferation was inhibited by berberine, the protein level of PKM2 was significantly downregulated and the mRNA level remained unaffected. We further found that berberine affected PKM2 spatial structure and promoted PKM2 ubiquitination, thus disrupting the equilibrium between synthesis and ubiquitination-mediated degradation of PKM2 in tumor cells and promoting its degradation. This is in line with previous observations that PKM2 is regulated by the ubiquitination pathway (Zheng et al., 2019; Kim et al., 2015), and confirms our hypothesis that berberine affects the stability of PKM2 through the level of post-translational modification of the protein. The high expression of PKM2 in tumor cells also promotes the phosphorylation of STAT3 into the nucleus, and the sustained activation of STAT3 up-regulates the expression of genes such as the apoptosis suppressor Bcl-2 and the cell cycle regulatory protein Cyclin D1, stimulating cell proliferation and inhibiting apoptosis (Nagasawa et al., 2020; Tang et al., 2018). In our experiments, the interaction between berberine and PKM2 leads to the negative regulation of

STAT3 phosphorylation, thereby inhibiting its activation, promoting apoptosis, and inhibiting the proliferation of colorectal cancer cells.

Despite the anti-colorectal cancer mechanisms of berberine that have been explored (Tong et al., 2020) and multiple targets and pathways, as well as transcriptional and post-translational interference, have been reported, how they interfere with the metabolic reprogramming of colorectal cancer cells has not been demonstrated. In our *in vivo* and *ex vivo* experiments, the inhibitory effect of berberine on metabolic reprogramming and proliferation of colorectal cancer cells was no longer observed when PKM2 was knocked down, which was restored after the overexpression of PKM2 homologous mutation. These results provide strong evidence that berberine analogs exert their anti-colorectal cancer effects mainly by acting directly on PKM2, a rate-limiting enzyme.

From our structural modeling, the binding sites of berberine in PKM2 were identified as F244 and I119, suggesting the mechanism of ubiquitination modification allosteria. It was found that F244A and I119S mutants eliminated the inhibitory effect of berberine on PKM2 by separating berberine from its active sites. This is demonstrated by both *in vitro* cell proliferation assay and *in vivo* tumor-bearing mice assay, in which berberine did not show a significant inhibitory effect on F244A and I119S mutant tumor cells. When the tumor cells with F244A or I119S mutant PKM2 were tested for thermal migration analysis, the expression of PKM2 in the berberine group was similar to that in the control group, indicating that berberine did not interact with F244A and I119S mutant colorectal cancer cells. In addition, biotinylated berberine was significantly reduced in the PKM2 expression region of F244A or I119S mutants by laser confocal microscopy; no berberine was detected in PKM2 by immunoprecipitation combined with MS. Therefore, we conclude that F244 and I119 sites are responsible for the changes in PKM2 ubiquitination induced by berberine. We also observed a small amount of ubiquitination of PKM2 in colorectal cancer cells, which is assumed to be in dynamic equilibrium. We further examined the co-expression of PKM2 and Stub1, which is a key ubiquitin ligase for PKM2 degradation (Shang et al., 2017). In contrast to PKM2 that the protein level was inhibited, the expression of Stub1 was unaffected by berberine, showing that the inhibitory effect of berberine by directly targeting PKM2 and resulting in changes in its spatial structure and promotion of its ubiquitination is independent of Stub1.

As a personalized method for drug sensitivity analysis, PDX model tumors are similar to primary tumors and have become an important tool for cancer transformation research (Yoshida, 2020; Qin et al., 2016). In our studies, three PDX tumors from different patients with high EXPRESSION of PKM2 were used to establish PDX models. Owing to the low oral bioavailability of berberine (Chen et al., 2011; Kheir et al., 2010), the intraperitoneal route was used based on literature (Wu et al., 2018; Li et al., 2015). Consistent with the *in vitro* results observed in colorectal cancer cell lines, berberine promoted PKM2 ubiquitination and inhibited PKM2 expression. PKM2 activity was down-regulated, and pyruvate and lactic acid production was reduced, indicating an inhibitory effect on metabolic reprogramming. The co-expression of PKM2 and P-STAT3 was also inhibited and the expression of Bcl-2 and Cyclin D1 was down-regulated.

The structural model of PKM2-berberine indicated that the inner oxygen ring and the N atomic ring are the key binding positions. Such N-*O*-O structure is observed in other anti-cancer drugs such as harringtonine and camptothecin when comparing their structures with that of berberine (see Figure S16, marked with an "*"). We, therefore, assume that the N-*O*-O triangular structure and the internal ammonium salt structure have a close relationship with the anti-tumor activity and the optimization of the structure-activity relationship by medicinal chemistry, combined with a more detailed structural analysis of PKM2-berberine interactions, would lead to novel drugs with better pharmacodynamics and pharmacokinetics. In this regard, without disrupting the N-*O*-O triangular structure and the internal ammonium salt structure, and the high expression of avidin of tumor cells, biotinylated berberine has a good inhibitory effect with EC_{50} of 3.47 μM. In addition, Boc-aminocaproic acid-berberine ester (Figure S17A) and *p*-aminobenzoic acid-berberine ester (Figure S18A) were synthesized to improve lipid solubility and characterized by MS, hydrogen NMR, and carbon NMR (Figures S19–S24). The EC_{50} values to inhibit tumor cells were 4.71 and 1.59 μM, respectively (Figures S17B and S18B). Compared with berberine (4.62 μM), the biological activity of *p*-aminobenzoic acid-berberine ester was improved to some extent. Our next plan is to open the benzene ring at the methoxy position or add an F atom to further optimize the structure and activity of berberine. Overall, the spatial structure of the berberine-PKM2 complex will help to finally reveal the

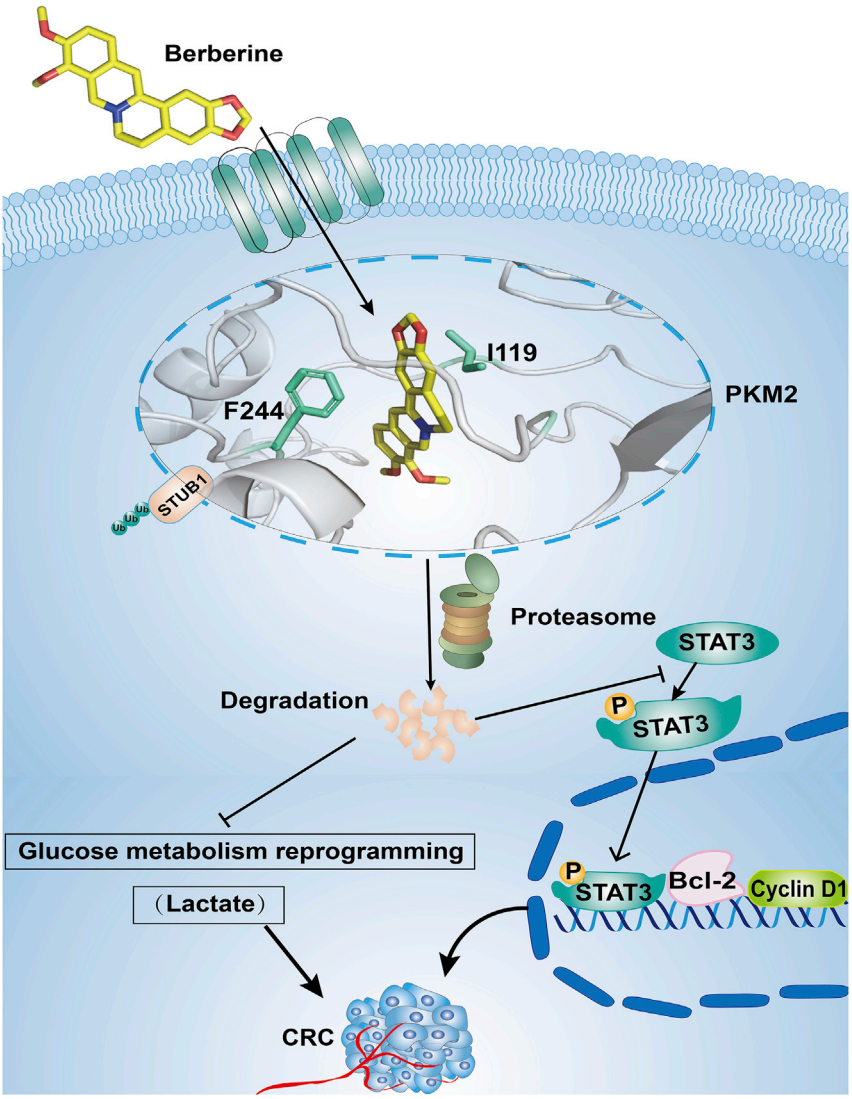

Figure 8. Illustration of the mechanism of berberine inhibition of colorectal cancer progression

Berberine enters the cell and directly targets PKM2. The N-*O*-O triangle structure of berberine contributes to hydrophobic interaction with I119 amino acid residues and π-π interaction with F244 amino acid residues of PKM2 protein, forming a sandwich-like overall structure, resulting in an increase in ubiquitination and degradation of PKM2. As a result, berberine further inhibits the reprogramming of glucose metabolism as well as the phosphorylation of STAT3, down-regulates the expression of Bcl-2 and cyclin D1 genes, suppresses cell proliferation, and promotes cell apoptosis, ultimately inhibiting the progression of colorectal cancer.

detailed mechanism of action of berberine analogs and make it possible to design new modulators of this key metabolic enzyme based on the structure.

In conclusion, berberine enters the cell and directly targets PKM2. Its N-*O*-O triangular structure contributes to the hydrophobic interaction with I119 amino acid residues and π-π interaction with F244 amino acid residues of PKM2 protein, forming an overall structure similar to a sandwich, thereby causing an increase in the ubiquitination and degradation of PKM2. As a result, berberine shows the inhibitory effect on both the reprogramming of glucose metabolism and the phosphorylation of STAT3, down-regulates the expression of Bcl-2 and Cyclin D1 genes, inhibits cell proliferation, promotes apoptosis, and inhibits the progression of colorectal cancer (Figure 8). Given the long history of the application of berberine in the practice of Traditional Chinese medicine and no major safety problems reported, we believe that berberine may be an ideal

candidate or lead compound for the prevention and treatment of colorectal cancer and other tumors with high PKM2 expression.

Limitations of the study

In addition to PKM2, our chemical proteomics analysis identified other proteins that may interact with berberine, and whether they are also involved in regulating other aspects of berberine in inhibiting intestinal cancer remains to be investigated.

STAR★METHODS

Detailed methods are provided in the online version of this paper and include the following:

- KEY RESOURCES TABLE
- RESOURCE AVAILABILITY
  - Lead contact
  - Materials availability
  - Data and code availability
- EXPERIMENTAL MODEL AND SUBJECT DETAILS
  - Cell culture
  - Patient specimens
- METHOD DETAILS
  - Cell viability assay
  - Animal studies
  - Synthesis and characterization of biotinylated berberine
  - Chemoprobe pull-down and chemo-proteomics
  - Cell lysis
  - Immunoprecipitation (IP)
  - Transient knockdown of H6PD, PKM2, MBP-1, and GAPDH
  - Stable PKM2 knockdown and PKM2 mutation overexpression
  - Western Blot
  - Immunofluorescence
  - Immunohistochemistry
  - Quantitative polymerase chain reaction (qPCR)
  - Sample extraction procedure and LC-MS/MS instrumentation and conditions
  - Cellular thermal shift assay (CETSA)
  - Computational details (Molecular docking and dynamics simulation)
  - Measurement of PKM2 activity, pyruvate and lactate
  - PET/CT
- QUANTIFICATION AND STATISTICAL ANALYSIS

SUPPLEMENTAL INFORMATION

Supplemental information can be found online at https://doi.org/10.1016/j.isci.2022.104773.

ACKNOWLEDGMENTS

This work was supported by the National Natural Science Foundation of China (21976080 and 21873045). We thank Dr Hong Huang and Yi-Zhuo Li for their help in the thesis scheme demonstration. We thank Dr Guo-Qiang Shao for his help in PET/CT testing and Dr Guo-Liang Dai for his help in determining berberine by MS.

AUTHOR CONTRIBUTIONS

Shi-Hai Yan contributed to the conception, design, acquisition, analysis, data interpretation, and article drafting. Li-Mu Hu contributed to molecular docking and dynamics simulation. Xue-Hui Hao contributed to the synthesis and characterization of berberine analogs. Jiang Liu provided human CRC tumors and non-tumor tissues. Xi-Yin Tan contributed to cell culture. Zhi-Rong Geng, Jing Ma, and Zhi-Lin Wang contributed equally to the conception, design, and supervision of the research. They gave final approval of the version to be submitted and any revised version.

DECLARATION OF INTERESTS

The authors declare no competing interests.

Received: March 18, 2022
Revised: May 13, 2022
Accepted: July 12, 2022
Published: August 19, 2022

REFERENCES

Abegg, D., Frei, R., Cerato, L., Prasad Hari, D., Wang, C., Waser, J., and Adibekian, A. (2015). Proteome-Wide profiling of targets of cysteine reactive small molecules by using ethynyl benziodoxolone reagents. Angew. Chem. Int. Ed. Engl. *54*, 10852–10857.

Bessi, I., Bazzicalupi, C., Richter, C., Jonker, H.R.A., Saxena, K., Sissi, C., Chioccioli, M., Bianco, S., Bilia, A.R., Schwalbe, H., and Gratteri, P. (2012). Spectroscopic, molecular modeling, and NMR-spectroscopic investigation of the binding mode of the natural alkaloids berberine and sanguinarine to human telomeric G-quadruplex DNA. ACS Chem. Biol. *7*, 1109–1119.

Bray, F., Ferlay, J., Soerjomataram, I., Siegel, R.L., Torre, L.A., and Jemal, A. (2018). Global cancer statistics 2018: GLOBOCAN estimates of incidence and mortality worldwide for 36 cancers in 185 countries. CA. Cancer. J. Clin. *68*, 394–424.

Case, D.A., Betz, R.M., Cerutti, D.S., Cheatham, T.E., Darden, T.A., III, Duke, R.E., Giese, T.J., Gohlke, H., Goetz, A.W., Homeyer, N., et al. (2016). AMBER 2016 (University of California).

Chen, C., Tao, C., Liu, Z., Lu, M., Pan, Q., Zheng, L., Li, Q., Song, Z., and Fichna, J. (2015). A randomized clinical trial of berberine hydrochloride in patients with diarrhea-predominant irritable bowel syndrom. Phytother Res. *29*, 1822–1827.

Chen, D., Dong, G., Noinaj, N., and Huang, R. (2019). Discovery of bisubstrate inhibitors for protein N-terminal methyltransferase 1. J. Med. Chem. *62*, 3773–3779.

Chen, D., Meng, Y., Yu, D., Noinaj, N., Cheng, X., and Huang, R. (2021). Chemoproteomic study uncovers HemK2/KMT9 as a new target for NTMT1 bisubstrate inhibitors. ACS Chem. Biol. *16*, 1234–1242.

Chen, W., Miao, Y.Q., Fan, D.J., Yang, S.S., Lin, X., Meng, L.K., and Tang, X. (2011). Bioavailability study of berberine and the enhancing effects of TPGS on intestinal absorption in rats. AAPS PharmSciTech *12*, 705–711.

Chen, X., Wang, Y., Ma, N., Tian, J., Shao, Y., Zhu, B., Wong, Y.K., Liang, Z., Zou, C., and Wang, J. (2020a). Target identification of natural medicine with chemical proteomics approach: probe synthesis, target fishing and protein identification. Signal Transduct. Target. Ther. *5*, 72.

Chen, Y.X., Gao, Q.Y., Zou, T.H., Wang, B.M., Liu, S.D., Sheng, J.Q., Ren, J.L., Zou, X.P., Liu, Z.J., Song, Y.Y., et al. (2020b). Berberine versus placebo for the prevention of recurrence of colorectal adenoma: a multicentre, double-blinded, randomised controlled study. Lancet. Gastroenterol. Hepatol. *5*, 267–275.

Christofk, H.R., Vander Heiden, M.G., Harris, M.H., Ramanathan, A., Gerszten, R.E., Wei, R., Fleming, M.D., Schreiber, S.L., and Cantley, L.C. (2008). The M2 splice isoform of pyruvate kinase is important for cancer metabolism and tumour growth. Nature *452*, 230–233.

Dai, G., Sun, B., Wu, L., Gao, X., Song, S., Sun, H., and Ju, W. (2018a). Comparative pharmacokinetics of three alkaloids in normal and acute hepatitis rats after oral administration of Yanhuanglian total alkaloids extract. Biomed. Chromatogr. *32*, e4329.

Dai, J., Liang, K., Zhao, S., Jia, W., Liu, Y., Wu, H., Lv, J., Cao, C., Chen, T., Zhuang, S., et al. (2018b). Chemoproteomics reveals baicalin activates hepatic CPT1 to ameliorate diet-induced obesity and hepatic steatosis. Proc. Natl. Acad. Sci. USA *115*, E5896–E5905.

Dai, L., Prabhu, N., Yu, L.Y., Bacanu, S., Ramos, A.D., and Nordlund, P. (2019). Horizontal cell biology: monitoring global changes of protein interaction states with the proteome-wide cellular thermal shift assay (CETSA). Annu. Rev. Biochem. *88*, 383–408.

Dayton, T.L., Gocheva, V., Miller, K.M., Israelsen, W.J., Bhutkar, A., Clish, C.B., Davidson, S.M., Luengo, A., Bronson, R.T., Jacks, T., and Vander Heiden, M.G. (2016). Germline loss of PKM2 promotes metabolic distress and hepatocellular carcinoma. Genes Dev. *30*, 1020–1033.

Facchin, C., Perez-Liva, M., Garofalakis, A., Viel, T., Certain, A., Balvay, D., Yoganathan, T., Woszczyk, J., De Sousa, K., Sourdon, J., et al. (2020). Concurrent imaging of vascularization and metabolism in a mouse model of paraganglioma under anti-angiogenic treatment. Theranostics *10*, 3518–3532.

Gao, X., Wang, H., Yang, J.J., Liu, X., and Liu, Z.R. (2012). Pyruvate kinase M2 regulates gene transcription by acting as a protein kinase. Mol. Cell. *45*, 598–609.

Goldberg, M.S., and Sharp, P.A. (2012). Pyruvate kinase M2-specific siRNA induces apoptosis and tumor regression. J. Exp. Med. *209*, 217–224.

Hosios, A.M., Fiske, B.P., Gui, D.Y., and Vander Heiden, M.G. (2015). Lack of evidence for PKM2 protein kinase activity. Mol. Cell. *59*, 850–857.

Israelsen, W.J., Dayton, T.L., Davidson, S.M., Fiske, B.P., Hosios, A.M., Bellinger, G., Li, J., Yu, Y., Sasaki, M., Horner, J.W., et al. (2013). PKM2 isoform-specific deletion reveals a differential requirement for pyruvate kinase in tumor cells. Cell *155*, 397–409.

Kheir, M.M., Wang, Y., Hua, L., Hu, J., Li, L., Lei, F., and Du, L. (2010). Acute toxicity of berberine and its correlation with the blood concentration in mice. Food. Chem. Toxicol. *48*, 1105–1110.

Kim, S.R., Kim, J.O., Lim, K.H., Yun, J.H., Han, I., and Baek, K.H. (2015). Regulation of pyruvate kinase isozyme M2 is mediated by the ubiquitin-specific protease 20. Int. J. Oncol. *46*, 2116–2124.

Kong, W., Wei, J., Abidi, P., Lin, M., Inaba, S., Li, C., Wang, Y., Wang, Z., Si, S., Pan, H., et al. (2004). Berberine is a novel cholesterol-lowering drug working through a unique mechanism distinct from statins. Nat. Med. *10*, 1344–1351.

Kotake, Y., Sagane, K., Owa, T., Mimori-Kiyosue, Y., Shimizu, H., Uesugi, M., Ishihama, Y., Iwata, M., and Mizui, Y. (2007). Splicing factor SF3b as a target of the antitumor natural product pladienolide. Nat. Chem. Biol. *3*, 570–575.

Kwon, S., and Chan, A.T. (2020). Extracting the benefits of berberine for colorectal cancer. Lancet. Gastroenterol. Hepatol. *5*, 231–233.

Laskowski, R.A., and Swindells, M.B. (2011). LigPlot+: multiple ligand-protein interaction diagrams for drug discovery. J. Chem. Inf. Model. *51*, 2778–2786.

Li, J., Zou, Y., Pei, M., Zhang, Y., and Jiang, Y. (2021a). Berberine inhibits the Warburg effect through TET3/miR-145/HK2 pathways in ovarian cancer cells. J. Cancer *12*, 207–216.

Li, P., Hao, Z., Liu, H., Zhu, B., Dang, L., Ma, C., Xu, Y., Zhang, Y., Fan, D., and Sun, S. (2021b). Quantitative proteomics analysis of berberine-treated colon cancer cells reveals potential therapy targets. Biology *10*, 250.

Li, W., Hua, B., Saud, S.M., Lin, H., Hou, W., Matter, M.S., Jia, L., Colburn, N.H., and Young, M.R. (2015). Berberine regulates AMP-activated protein kinase signaling pathways and inhibits colon tumorigenesis in mice. Mol. Carcinog. *54*, 1096–1109.

Li, Y.h., Li, X.f., Liu, J.t., Wang, H., Fan, L.L., Li, J., and Sun, G.P. (2018). PKM2, a potential target for regulating cancer. Gene *668*, 48–53.

Mao, L., Chen, Q., Gong, K., Xu, X., Xie, Y., Zhang, W., Cao, H., Hu, T., Hong, X., and Zhan, Y.Y. (2018). Berberine decelerates glucose metabolism via suppression of mTOR-dependent HIF-1α protein synthesis in colon cancer cells. Oncol. Rep. *39*, 2436–2442.

Martinez Molina, D., Jafari, R., Ignatushchenko, M., Seki, T., Larsson, E.A., Dan, C., Sreekumar, L., Cao, Y., and Nordlund, P. (2013). Monitoring drug target engagement in cells and tissues using the cellular thermal shift assay. Science *341*, 84–87.

Nagasawa, I., Muroi, M., Kawatani, M., Ohishi, T., Ohba, S.I., Kawada, M., and Osada, H. (2020). Identification of a small compound targeting PKM2-regulated signaling using 2D gel electrophoresis-based proteome-wide CETSA. Cell. Chem. Biol. *27*, 186–196.e4.

Qin, X., Wang, X., Liu, F., Morris, L.E., Wang, X., Jiang, B., and Zhang, Y. (2016). Gankyrin activates mTORC1 signaling by accelerating TSC2 degradation in colorectal cancer. Cancer. Lett. *376*, 83–94.

Ru, J., Li, P., Wang, J., Zhou, W., Li, B., Huang, C., Li, P., Guo, Z., Tao, W., Yang, Y., et al. (2014). TCMSP: a database of systems pharmacology for drug discovery from herbal medicines. J. Cheminf. *6*, 13.

Shang, Y., He, J., Wang, Y., Feng, Q., Zhang, Y., Guo, J., Li, J., Li, S., Wang, Y., Yan, G., et al. (2017). CHIP/Stub1 regulates the Warburg effect by promoting degradation of PKM2 in ovarian carcinoma. Oncogene *36*, 4191–4200.

Spradlin, J.N., Hu, X., Ward, C.C., Brittain, S.M., Jones, M.D., Ou, L., To, M., Proudfoot, A., Ornelas, E., Woldegiorgis, M., et al. (2019). Harnessing the anti-cancer natural product nimbolide for targeted protein degradation. Nat. Chem. Biol. *15*, 747–755.

Su, K., Hu, P., Wang, X., Kuang, C., Xiang, Q., Yang, F., Xiang, J., Zhu, S., Wei, L., and Zhang, J. (2016). Tumor suppressor berberine binds VASP to inhibit cell migration in basal-like breast cancer. Oncotarget *7*, 45849–45862.

Tang, J.C., Ren, Y.G., Zhao, J., Long, F., Chen, J.Y., and Jiang, Z. (2018). Shikonin enhances sensitization of gefitinib against wild-type EGFR non-small cell lung cancer via inhibition PKM2/stat3/cyclinD1 signal pathway. Life. Sci. *204*, 71–77.

Tong, M., Liu, H., Hao, J., and Fan, D. (2020). Comparative pharmacoproteomics reveals potential targets for berberine, a promising therapy for colorectal cancer. Biochem. Biophys. Res. Commun.. S0006–291X(20)30320-X.

Trott, O., and Olson, A.J. (2010). AutoDock Vina: improving the speed and accuracy of docking with a new scoring function, efficient optimization and multithreading. J. Comput. Chem. *31*, 455–461.

Wang, W., and Kollman, P.A. (2000). Free energy calculations on dimer stability of the HIV protease using molecular dynamics and a continuum solvent model. J. Mol. Biol. *303*, 567–582.

Waterhouse, A., Bertoni, M., Bienert, S., Studer, G., Tauriello, G., Gumienny, R., Heer, F.T., de Beer, T.A.P., Rempfer, C., Bordoli, L., et al. (2018). SWISS-MODEL: homology modelling of protein structures and complexes. Nucleic. Acids. Res. *46*, W296–W303.

Weiser, J., Shenkin, P.S., and Still, W.C. (1999). Approximate atomic surfaces from linear combinations of pairwise overlaps (LCPO). J. Comput. Chem. *20*, 217–230.

Wong, N., Ojo, D., Yan, J., and Tang, D. (2015). PKM2 contributes to cancer metabolism. Cancer. Lett. *356*, 184–191.

Wu, Y.Y., Li, T.M., Zang, L.Q., Liu, B., and Wang, G.X. (2018). Effects of berberine on tumor growth and intestinal permeability in HCT116 tumor-bearing mice using polyamines as targets. Biomed. Pharmacother. *107*, 1447–1453.

Yang, P., Li, Z., Fu, R., Wu, H., and Li, Z. (2014). Pyruvate kinase M2 facilitates colon cancer cell migration via the modulation of STAT3 signalling. Cell. Signal. *26*, 1853–1862.

Yi, C.M., Yu, J., Kim, H., Lee, N.R., Kim, S.W., Lee, N.J., Lee, J., Seong, J., Kim, N.J., and Inn, K.S. (2017). Identification of actin as a direct proteomic target of berberine using an affinity-based chemical probe and elucidation of its modulatory role in actin assembly. Chem. Commun. *53*, 7045–7047.

Yoshida, G.J. (2020). Applications of patient-derived tumor xenograft models and tumor organoids. J. Hematol. Oncol. *13*, 4.

Zhang, Y., Li, X., Zou, D., Liu, W., Yang, J., Zhu, N., Huo, L., Wang, M., Hong, J., Wu, P., et al. (2008). Treatment of type 2 diabetes and dyslipidemia with the natural plant alkaloid berberine. J. Clin. Endocrinol. Metab. *93*, 2559–2565.

Zheng, Y.L., Li, L., Jia, Y.X., Zhang, B.Z., Li, J.C., Zhu, Y.H., Li, M.Q., He, J.Z., Zeng, T.T., Ban, X.J., et al. (2019). LINC01554-Mediated glucose metabolism reprogramming suppresses tumorigenicity in hepatocellular carcinoma via downregulating PKM2 expression and inhibiting Akt/mTOR signaling pathway. Theranostics *9*, 796–810.

STAR★METHODS

KEY RESOURCES TABLE

REAGENT or RESOURCE	SOURCE	IDENTIFIER
Antibodies		
Anti-PKM2 antibody	Cell Signal Technology	#4053
PKM2-specific Monoclonal antibody	proteintech	60268-1-Ig
Anti-Bcl-2 antibody	Affinity Biosciences LTD	AF6139
Anti-Cyclin D1 antibody	Affinity Biosciences LTD	AF0931
Phospho-STAT3 (Tyr705) Antibody	Affinity Biosciences LTD	AF3293
Anti-STAT3 antibody	Affinity Biosciences LTD	AF6294
Anti-Stub1 antibody	abcam	ab134064
Anti-Ubiquitin antibody	abcam	ab134953
Anti-Ki67 antibody	abcam	ab16667
Chemicals, peptides, and recombinant proteins		
Berberine	Shanghai yuanye Bio-Technology Co., Ltd	2086-83-1
MG132	MedChemExpress LLC	133,407-82-6
Dynabeads M−280 Streptavidin	ThermoFisher Scientific	#11205D
Critical commercial assays		
CCK8	Beyotime Biotechnology	C0038
Annexin V-FITC apoptosis Detection Kit	Beyotime Biotechnology	C1062L
Cell Cycle and Apoptosis Detection Kit	Beyotime Biotechnology	C1052
Experimental models: Cell lines		
HT29	ATCC	#HTB-38
HCT116	ATCC	#CCL-247
Experimental models: Organisms/strains		
Mouse: Nu/Nu mice	Charles River	N/A
Mouse: NCG mice	GemPharmatech Co., Ltd.	N/A
Oligonucleotides		
See Table S6 for oligonucleotide information	This paper	N/A
Software and algorithms		
GraphPad Prism version 6.0	GraphPad Software	https://www.graphpad.com/
Image-Pro 6.0	NIH	https://sybyl-x.software.informer.com/2.0/
CFX ManagerTM version 2.1	Bio-Rad	N/A

RESOURCE AVAILABILITY

Lead contact

Further information and requests for resources and reagents should be directed to and fulfilled by the lead contact (gengzr@nju.edu.cn).

Materials availability

Mice and reagents generated in this study are available by request to the lead contact (gengzr@nju.edu.cn).

Data and code availability

All data produced in this study are included in the published article and its supplemental information, or are available from the lead contact upon request. This paper does not report original code. Any additional

information required to reanalyze the data reported in this paper is available from the lead contact upon request.

EXPERIMENTAL MODEL AND SUBJECT DETAILS

Cell culture

HT29 (#HTB-38) and HCT16 cells (#CCL-247) were obtained from ATCC. All the cell lines were cultured according to the provider's recommendations.

Patient specimens

Tissue collection was approved by the Medical Ethical Committee of the Affiliated Hospital of Nanjing University of Chinese Medicine. Fresh and paraffin-embedded colorectal cancer blocks were collected from patients undergoing surgery at the Affiliated Hospital of Nanjing University of Chinese Medicine with informed consent.

METHOD DETAILS

Cell viability assay

Cells were seeded at a density of 1×10^4 cells/well in 96-well plates under the condition of high glucose (4.5 g/L). Cell viability was determined 24 h after the addition of berberine or biotinylated berberine by CCK8 (Beyotime Biotechnology) according to the manufacturer's instruction. Absorbance was measured in a plate reader at 450 nm. Fractional survival was plotted against the logarithm of drug dose, and EC_{50} values were calculated by Prism software (GraphPad Software).

Animal studies

All animal experiments were approved by the Medical Ethical Committee of the Affiliated Hospital of Nanjing University of Chinese Medicine. Mice were housed in a sterile environment with micro isolator cages and allowed access to water and chow *ad libitum*. Cell line xenografts were established by subcutaneously injecting 4×10^6 HT29 cells into the axilla of 5-6-week-old male Nu/Nu mice (Charles River).

PDX tumors were established and propagated in 5-6-week-old male NOD/ShiLtJGpt-Prkdc^{em26}Il2rg^{em26}/Gpt (NCG) mice (GemPharmatech Co., Ltd.) as described. PDX1 was established using microsatellite stable (MSS) tumor fragments (T3N0M0) taken from the sigmoid colon of a 52-year-old female. PDX2 was established using MSS tumor fragments (T4N1M0) taken from the sigmoid colon of a 71-year-old male. PDX3 was established using MSS tumor fragments (T3N0M0) taken from the right colon of a 54-year-old male. Xenograft tumors reached 3–6 mm in size before treatment.

Tumor-bearing mice were randomized into different groups of 6 mice each and treated with berberine (10 mg/kg). Calipers monitored tumor growth, and tumor volumes were calculated according to the formula $1/2 \times \text{length} \times \text{width}^2$. The ethical endpoint was defined as a time point when a tumor reached 1.5 cm or more in any dimension. Tumor tissues were dissected and fixed in 10% formalin and embedded in paraffin.

Synthesis and characterization of biotinylated berberine

For berberrubine biosynthesis, a high-temperature lysis method was used. Berberine (2.00 g, 5.390 mmol) was weighed on a weighing balance and placed in a 250 ml round-bottom flask, from which the air was pumped out. The flask was placed in an oil bath and heated with shaking at 196°C for 20 min until all the yellow solid changed to dark red, and 100 ml of mixed solvent (5:95 mixture of ethanol and hydrochloric acid, *v/v*) was added to acidify the content after cooling at room temperature, and distilled under reduced pressure to obtain a red solid (1.66 g, 4.639 mmol), namely, berberrubine with a yield of 86.1%.

Synthesis of biotin-N-hydroxysuccinimide activated ester: To a 250 ml three-necked flask, biotin (5 g, 20.484 mmol) and 1-(3-dimethylaminopropyl)-3-ethylcarbodiimide hydrochloride (5.79 g, 30.203 mmol) were added and dissolved in 100 ml N, N-dimethylformamide (DMF) under stirring, and then N-hydroxysuccinimide (2.83 g, 24.589 mmol) and 4-dimethylaminopyridine (1.16 g, 0.949 mmol) were added and stirred at room temperature for 24 h before spun dry. 150 ml isopropanol was added to the remaining residue. The mixture was sonicated to dissolve and refrigerated at 4 °C overnight, filtered, and dried to obtain a solid white, namely, biotin-N-hydroxysuccinimide activated ester (5.64 g, 16.535 mmol) with a yield of 80.7%.

Synthesis of 6-biotin aminohexanoic acid: To a 250 ml three-necked flask, biotin-N-hydroxysuccinimide activated ester (1.50 g, 4.397 mmol) and 6-aminohexanoic acid (0.70 g, 5.337 mmol) was added and dissolved in 30 ml DMF under stirring, and then 1.5 ml triethylamine was added under an ice bath. After the reaction was carried out at room temperature for 24 h, the mixed solution was spun dry. 80 ml of water and 10 ml of formic acid were then added to the remaining residue, and the pH was adjusted to 6. The mixture was dissolved by ultrasonication and refrigerated at 4 °C overnight, and a white solid was precipitated, filtered and dried to obtain 6-biotinylaminohexanoic acid (1.30 g, 3.640 mmol) with a yield of 82.8%.

Synthesis of biotin-aminocaproic acid-berberine esters: To a 100 ml three-necked flask, 6-biotin-aminocaproic acid (1.11 g, 3.108 mmol) and 1-(3-dimethylaminopropyl)-3-ethylcarbodiimide hydrochloride (0.67 g, 3.495 mmol) were added and dissolved in 10 ml DMF under stirring, and then berberine (0.92 g, 2.576 mmol) dissolved in 20 ml DMF and 4-dimethylaminopyridine (0.03 g, 0.246 mmol) were added under an ice bath. The resulting mixed solution was reacted at room temperature for 36 h. After completion of the reaction, the solvent was removed by distillation under reduced pressure. The crude product was purified by silica gel column chromatography (1:8 mixture of methanol and dichloromethane, *v/v*) to give a red solid (1.01 g, 1.451 mmol), namely, biotin-aminocaproic acid-berberine ester (compound 2) with a yield of 46.7%.

Chemoprobe pull-down and chemo-proteomics

250 μL of Dynabeads M-280 Streptavidin (ThermoFisher Scientific; #11205D) were washed 3 times and resuspended in 250 μL PBS. 350 μg of native protein extract (containing the biotinylated probe) was added and incubated for 30 minutes at room temperature with gentle rotation. The chemoprobe complex bound to the streptavidin beads was separated using a magnet and washed 4 times in PBS. After the last wash, the bound proteins were eluted with the incubation of glycine buffer (pH 2.5–3.0) for 20 min. The mixture was centrifuged for 20 min at room temperature at 15000 g. The supernatant after centrifugation was collected and neutralized with 1 M tris buffer (pH 8.0). The sample was reduced, alkylated and digested with trypsin (m/m 1:50) at 37°C for 20 h. The digested product was desalted, lyophilizated and reconstituted in 0.1% FA solution. The sample was loaded to the trap column by the automatic sampler with 1 h gradient elution. After each full scan, up to 20 product ion scans were collected. Proteins were homologously searched according to the *Homo Sapiens* protein database with proteome discoverer 1.4 software. KEGG analysis was carried out through Omicshare platform (Omicshare, http://www.omicshare.com/tools/).

Cell lysis

Cells were lysed in 1X Cell Lysis Buffer (Cell Signaling; #9803) containing 1X Complete Mini Protease Inhibitor Cocktail Tablets (ROCHE; #11836153001) and biotinylated probe (25 nM for ELISA or 5 μM for chemoprobe pull-down) was added to frozen cell pellets containing 1×10^6 cells. Tubes were incubated for 5 min on ice and briefly sonicated to achieve lysis. The resulting extracts were centrifuged for 10 min at 14000 rpm at 4°C. According to the manufacturer's instructions, supernatants were collected and quantified by Bradford assay (BIO-RAD; #500-0006).

Immunoprecipitation (IP)

Anti-PKM2 antibody (Cell Signaling Technology; #4053) diluted 1:25 in PBS, was added to native protein extraction or rKDM1A (Active Motif; #31334) and incubated overnight (O/N) at 4°C with gentle rocking. 50 μl of Protein A Magnetic Beads (Cell Signaling; #8687) were washed with 500 μL 1x Cell Lysis Buffer (Cell Signaling; #9803) and the supernatant was removed using a magnet.

Lysate preincubated with primary antibody (immune-complex) was then added to magnetic bead pellet. Cross-link reaction was performed with gentle rocking for 30 min at room temperature (RT). Protein A magnetic beads not bound to immunocomplex were removed by washing 3 times. The resulting pellet was resuspended in 25 μL of 3 x sodium dodecyl sulfate (SDS) sample buffer and stored at −20°C.

Transient knockdown of H6PD, PKM2, MBP-1, and GAPDH

HT29 cell lines were transiently transfected with shRNA plasmids. Plasmids were constructed, packed, and purified by Genechem (Shanghai, China), and were processed according to the protocol provided by the manufacturer. The sequences of the oligonucleotides can be found in the Table S4.

Stable PKM2 knockdown and PKM2 mutation overexpression

PKM2 knockdown HT29 cell lines were transfected stably with the shRNA Lentivirus. Cell cultures were maintained under neomycin selection for 2 weeks to generate stable shRNA-expressing cells. The sequences of the oligonucleotides can be found in the Table S4.

Lentiviral CMV enhancer-MCS-3FLAG-EF1a-ZsGreen1-T2A-puromycin PKM2 (NM_002654-homologous mutation), PKM2 (NM_002654 (I119S)-mutation) or PKM2 (NM_002654 (F244A)-mutation) plasmids and Lentiviruses were constructed, packed, and purified by Genechem (Shanghai, China), and were processed according to the protocol provided by the manufacturer. For the generation of stable over-expressing cells, cell cultures were maintained under puromycin selection for 2 weeks.

PKM2 (Homologous mutation)

388aa-394aa

The sequences of WT: GCCATCTACCACTTGCAATTA

The sequences of Homologous mutation: GCAATATATCATTTACAGTTG

PKM2 (I119S mutation)

119aa

The sequences of WT: ATC

The sequences of Locus mutation: AGC

PKM2 (F244A mutation)

244aa

The sequences of WT: TTC

The sequences of Locus mutation: GCC

Western Blot

Western blotting assays were carried out using standard procedures. The antibodies included anti-PKM2, p-STAT3, STAT3, bcl-2, cyclin D1, and PKM1 (Table S5). Antibodies for horseradish peroxidase-conjugated goat anti-rabbit/anti-mouse IgG and β-actin were purchased from Sigma (St. Louis, MO, USA).

Immunofluorescence

For immunofluorescence staining, cells or cross-sections of tissues were treated with anti-PKM2, p-STAT3, or biotin overnight at 4 °C, and secondary Fluor Ab was used to detect the signal.

Immunohistochemistry

Immunohistochemistry for Ki67 was performed using the tumor sections obtained from nude mice xenografts. Slides containing the sections were stained with antibodies against Ki67. After microwaving 3 times for 5 min, endogenous peroxidase was neutralized with 3% hydrogen peroxidase in methanol for 15 min at room temperature and primary antibodies were applied at 4°C overnight. Anti-rabbit IgG biotinylated secondary antibody was applied for 30 min at 37°C followed by SA-HRP for 30 min at 37°C. Peroxidase was visualized using DAB for 5 min and counterstained in Mayer's hematoxylin for 20 min.

Quantitative polymerase chain reaction (qPCR)

The total RNA was extracted by using Trizol (Ambion, USA). The High Capacity cDNA Reverse Transcription Kit (Vazyme, Nanjing, China) was used to conduct the reverse transcription. Thermo Fisher Scientific synthesized the primers, and the primer sequences are summarized in the Table S6. SYBR Green chemistry (Vazyme, Nanjing, China) on a 7500 fast RT-PCR system was used to perform an amplified reaction. The amount of target, normalized to an endogenous reference (β-actin), was given by the $2^{-\Delta\Delta CT}$ calculation.

Sample extraction procedure and LC-MS/MS instrumentation and conditions

All samples were thawed at room temperature before analysis. A 50 μL aliquot of IP PKM2 protein was transferred into a 1.5 mL centrifuge tube, and 10 μL of IS working solution (1.4 μg mL^{-1}) and 150 μL

acetonitrile were added. The mixture was vortexed for 3 min and then centrifuged at 12,000 rpm for 10 min. Subsequently, 5 μL supernatant was injected onto the LC-MS/MS system for analysis.

Analyses were performed with ACQUITY Ultra Performance LC chromatography System (Waters, USA) consisting of a quat pump, an auto-sampler and an online degasser. The chromatographic separation was performed on an Agilent ZOBAX SB C18 column (4.6 mm × 150 mm, 5 μm). The mobile phase consisted of acetonitrile-0.1% formic acid (45:55, *v/v*) at a flow rate of 0.25 mL/min. The auto-sampler temperature was maintained at 4°C and the injection volume was 5 μL. The total LC run time was 3 min with the column temperature kept at 40°C.

The berberine and tetrahydropalmatine (IS) were detected using a Quattro Premier mass spectrometer (Waters, USA) with an electrospray ionization (ESI) interface in positive ion mode. Multiple reaction monitoring (MRM) was used to monitor precursor to production transition of *m/z* 336.2→320.0 for berberine, and *m/z* 356.1→191.9 for IS. The analytical data were processed using MassLynx software (version 1.4, Waters).

For the analyte and IS, the source parameters were set as follows: capillary voltage, 3500 V; desolvation temperature, 350°C; source temperature, 120°C; desolvation gas flow, 600 L/h, and cone gas flow, 30 L/h. The compound-dependent parameters such as cone voltage and collision energy were optimized at 30 V and 32 eV for berberine, and 30 V and 32 eV for IS, respectively. Quadrupole 1 and quadrupole 3 were maintained at unit resolution. The dwell time was 200 ms for both the analyte and IS.

Cellular thermal shift assay (CETSA)

The binding of berberine to endogenous PKM2 was analyzed by CETSA based on a published protocol. Briefly, cells were treated with berberine or control (0.1% DMSO) for 2 hours in T-75 flasks. After treatment, cells were harvested, washed once with 1× PBS, resuspended in 750 μL HBSS, and lysed by 4 cycles of freezing (dry ice/ethanol for 5 min) and thawing (37°C for 5 min). Samples were then aliquoted equally into 0.2-mL PCR tubes and heated at different temperatures for 3 min on a thermal cycler (Hybaid), followed by centrifugation at 13,200× rpm for 5 min. The supernatants were analyzed by western blotting.

Computational details (Molecular docking and dynamics simulation)

The three-dimensional structure of the PKM2-berberine complex was derived using the best-scoring binding mode given by AutoDock Vina software. MD simulations were then performed to examine the structure of the ligand and its surrounding residues at a distance of about 4 Å by for the first and last frames (i.e., at 80 ns) and to obtain the amino acid-berberine interaction mode separately, recording the evolution of the spacing of the atom pairs they contain over time.

In the molecular dynamic simulations, the force field parameters of the protein were selected as the ff99sb and ff14sb force field of AMBER16 software package (Case et al., 2016) and the force field parameters of the ligand were selected as GAFF (general AMBER force field). The TIP3PBOX water model was used, and the surface of the water box was 10 Å away from the protein. The 150 mM of sodium and chloride ions were added to the system to maintain the salt concentration to simulate the real physiological environment. The entire system contains about 72,000 water molecules (about 216,000 atoms), one protein molecule (about 15,900 atoms), and one ligand molecule (43 atoms), for a total of about 232,000 atoms. The integration step was set to 2 fs, and the SHAKE algorithm was used to constrain all bonds containing H atoms. The temperature and pressure control methods used were Langevin thermostat and Berendsen Barostat, respectively. The heat bath coupling time constant and pressure relaxation time of the system was set to 2 ps. The output frequency of the MD trajectory was 10 ps.

The protein α-carbon atoms were first confined (binding constant was set to 5.0 kcal/mol/A^2), and the system was energy minimized using the steepest descent method (20,000 steps). The system was equilibrated by first keeping the protein α-carbon atoms constrained and ramping up the system temperature from 100 K to 300 K (100 ps), after which the temperature and pressure were maintained at 300 K and 1 atm, respectively, and all constraints were removed for kinetic sampling. The duration of the MD sampling was 80 ns. The evolution of the distances of amino acids I119, V209, N210, V216, F244, and berberine molecules with time was recorded separately. The possible modes of interaction of these amino acids with berberine molecules were analyzed.

MM/PBSA was used to calculate the binding free energies from the MD trajectories of the original berberine-3gr4 complex and its mutants. In MM/PBSA, the binding free energy (ΔG_{bind}) between a ligand and a receptor to form a complex is calculated as

$$\Delta G_{bind} = \Delta H - T\Delta S \approx \Delta E_{MM} + \Delta G_{sol} - T\Delta S$$
$$\Delta E_{MM} = \Delta E_{internal} + \Delta E_{electrostatic} + \Delta E_{vdw}$$
$$\Delta G_{sol} = \Delta G_{PB} + \Delta G_{SA}$$

where ΔE_{MM}, ΔG_{sol} and $-T\Delta S$ are the changes of the gas phase MM energy, the solvation free energy, and the conformational entropy upon binding, respectively. The ΔE_{MM} term includes $\Delta E_{internal}$, $\Delta E_{electrostatic}$, and ΔE_{vdw} (*van der Waals*) energies. The ΔG_{solv} is the sum of electrostatic solvation energy (polar contribution), ΔG_{PB}, and the non-electrostatic solvation component (nonpolar contribution), ΔG_{SA}. PB model is used to calculate the polar contribution, while solvent accessible surface area (SASA) is used to estimate the nonpolar energy. The conformational entropy change was neglected in our calculations.

To reduce noise in the simulations, single trajectory approach was chosen to cancel $\Delta E_{internal}$ between ligand, receptor and complex. Then the gas-phase interaction energy between the protein and the ligand, ΔE_{MM}, is the sum of electrostatic and van der Waals interaction energies. The solvation free energy $\Delta G_{solvation}$ is the sum of polar (ΔG_{PB}) and nonpolar (ΔG_{SA}) parts. The ΔG_{PB} term was calculated by numerically solving the finite-difference Poisson-Boltzmann equation using *pbsa* program included with AmberTools. The atomic radii were set up according to the prmtop files. The ionic strength (in Molarity) was set to 0.15. The value of the exterior dielectric constant was set to 80, and the solute dielectric constant was set to one of three values: 1, 2, or 4 (Wang and Kollman, 2000). The nonpolar contribution was determined based on SASA using LCPO method (Weiser et al., 1999). $\Delta G_{SA} = 0.005 \times \Delta SASA$. Calculations of ΔE_{MM}, ΔG_{PB}, and ΔG_{SA}, used 200 snapshots that evenly extracted from the last 2 ns of the single MD trajectory of complex.

Measurement of PKM2 activity, pyruvate and lactate

PKM2 activity was measured based on the generation of pyruvate, which was oxidized by pyruvate oxidase and produced a color change (λ = 570 nm). Assay of PKM2 activity followed the protocol of the PKM2 Activity Colorimetric/Fluorometric Assay Kit (Biovision).

According to the manufacturer's instructions, lactate and pyruvate were measured using an assay kit (Nanjing Jiancheng Bioengineering Institute, Nanjing, China). Cells or tissues were mechanically homogenized in pyruvate assay buffer (1 mg/5 μL buffer). After extracts were clarified by centrifugation (20,000g, 4°C, 20 min, ×2), the supernatant was used for the assay. 1×10^6 cells were lysed in the corresponding buffer for assay.

PET/CT

Mice-bearing xenografts were subjected to ^{18}F-FDG micro-PET/CT analysis performed on an Inveon MM Platform (Siemens, Munich, Germany). Mice were anesthetized with 2% isoflurane before ^{18}F-FDG injection (a single injection of 3.7–7.4 MBq/0.1 mL ^{18}F-FDG via tail vein). 40 min after administration of the tracer, mice were placed on the PET scanner bed and were maintained under continuous anesthesia during the study. Inveon Acquisition Workplace (Siemens) was used for scanning. 3D regions of interest were drawn over the entire tumor guided by CT images, and tracer uptake was measured using Inveon Research Workplace software. The SUV was calculated as decay-corrected activity (kBq) per milliliter of tissue volume/injected ^{18}F-FDG activity (kBq) per gram of body weight.

QUANTIFICATION AND STATISTICAL ANALYSIS

The data are presented as the mean ± SD All results are representative of at least three independent experiments. The differences were analyzed by Fisher exact test for categorical variables and by *Student's t test* for continuous variables using SPSS 16.0 software (SPSS, Chicago, IL, USA). Differences with a p value <0.05 (denoted by *) are considered significant (**$p < 0.01$ and *$p < 0.05$).